AIAA JOURNAL
Vol. 48, No. 1, January 2010

Characteristics of the Shock Noise Component of Jet Noise

K. Viswanathan,* M. B. Alkislar,† and M. J. Czech‡
The Boeing Company, Seattle, Washington 98124-2207

DOI: 10.2514/1.38521

The characteristics of the flow and the noise of shock-containing jets have been studied for nearly three decades. It is now established that broadband shock-associated noise is generated by the interaction of the downstream-convecting coherent structures of the jet flow with the shock cells in the jet plume. Past analyses of far-field data have been carried out with the total measured noise, which contains both the turbulent mixing noise and shock noise. In this study, these two components are first separated and extracted from the total spectra. Both convergent and convergent-divergent nozzles are considered. The decomposition is made possible by a recently developed scaling methodology for turbulent mixing noise, which provides excellent collapse of the mixing noise spectra from jets at all velocities but at a fixed temperature ratio. The characteristics of the shock component alone are investigated. A surprising effect of jet temperature on shock noise is established for the first time: the levels increase as the jet is first heated; however, the levels do not increase with further increase in jet temperature. The physical phenomenon responsible for this saturation of levels is not known at this time. The intensity for shock noise in the forward quadrant does not scale as the fourth power (shock exponent) of

$$\sqrt{|M_j^2 - M_D^2|}$$

but spans a range from 2.9 to 6.17, depending on the radiation angle and the jet temperature ratio. It is not straightforward to collapse the shock spectra. It is also established for the first time that nonlinear propagation effects are manifested at lower radiation angles, in which the shock component is dominant. The physical phenomenon that triggers the onset of nonlinear propagation for the shock noise could not be identified. The characteristics of the correlation functions at the lower inlet angles for subsonic and supersonic jets are different, attesting to the different noise generation mechanisms.

I. Introduction

SHOCK-ASSOCIATED noise is generated when a convergent-divergent nozzle is operated at offdesign Mach numbers, and when a convergent nozzle is operated at supercritical nozzle pressure ratios. Under these conditions, shocks are established in the jet plume due to incorrect expansion and the consequent mismatch between the static pressure in the jet and the ambient medium. These shocks generate two components of noise, broadband and discrete tones. The intensity of shock-associated noise is dependent on the degree of mismatch between the design Mach number (M_d) and the fully expanded jet Mach number (M_j). The relative importance of the broadband shock-associated noise and turbulent mixing noise is a strong function of radiation angle and jet operating conditions. The broadband shock component is usually dominant at the lower inlet angles, in which the level of the turbulent mixing noise is low; the mixing noise is radiated principally to the aft directions.

Many of the characteristics of broadband shock-associated noise have been studied for the past three decades, since the pioneering experimental work of Harper-Bourne and Fisher [1]. They developed the first semi-empirical noise model for the broadband component of shock-associated noise. Their work was based on analysis of far-field spectral directivity and was supported with turbulence measurements in underexpanded jets using the crossed beam laser schlieren technique. Subsequently, Tanna [2], Seiner and Norum [3,4], Norum and Seiner [5,6], Tam and Tanna [7], Seiner [8], Seiner and Yu [9] and Yamamoto et al. [10] carried out extensive noise studies, including offdesign measurements from convergent-divergent (CD) nozzles, that have extended our understanding of broadband shock-associated noise. The experiments at NASA Langley Research Center by Seiner, Norum and Yu concentrated on the aerodynamic characteristics,

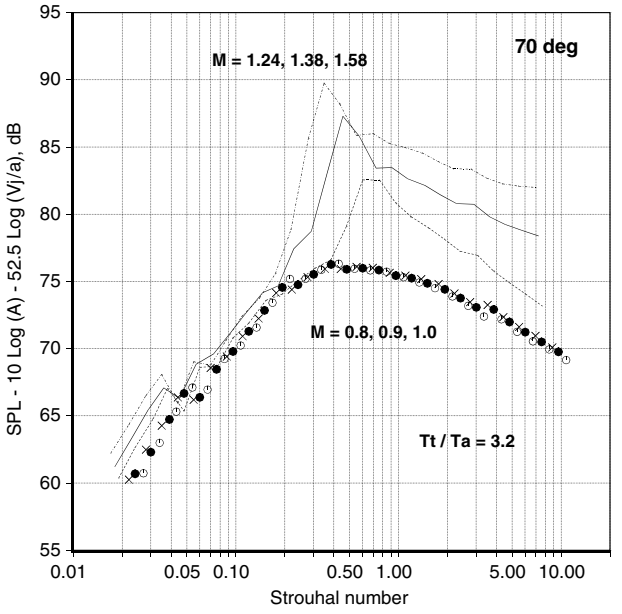

Fig. 1 Normalized one-third octave spectra from heated jets at 70 deg: $T_t/T_a = 3.2$, $D = 2.45$ in. Symbols: subsonic Mach numbers, and lines: supersonic Mach numbers. Velocity exponent $n = 5.25$.

Presented as Paper 2835 at the 14th AIAA/CEAS Aeroacoustics Conference, Vancouver, BC, Canada, May 2008; received 12 May 2008; revision received 7 June 2009; accepted for publication 19 Sept. 2009.

*Boeing Technical Fellow, MS 67-ML, PO Box 3707; k.viswanathan@boeing.com. Associate Fellow AIAA.

†Aeroacoustics Engineer, MS 67-ML, PO Box 3707; mehmet.b.alkislar@boeing.com. Member AIAA.

‡Aeroacoustics Engineer, MS 67-ML, PO Box 3707; michael.j.czech@boeing.com. Member AIAA.

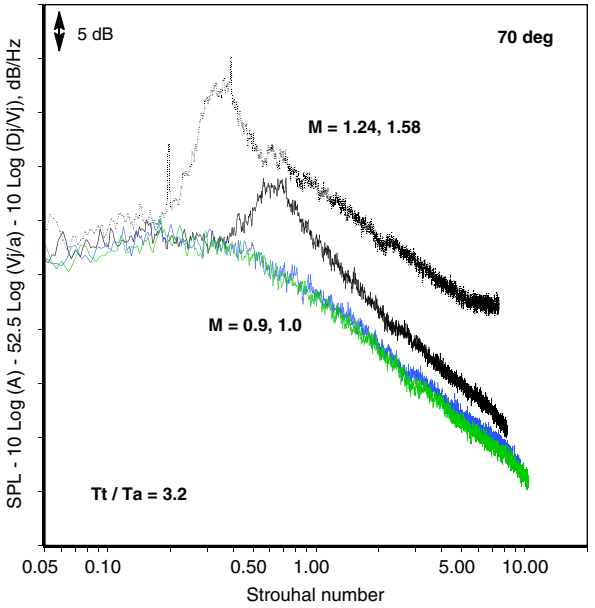

Fig. 2 Normalized narrowband spectra from heated jets at 70 deg: $T_t/T_a = 3.2, D = 2.45$ in. Blue and green: subsonic Mach numbers, and black lines: supersonic Mach numbers. Velocity exponent $n = 5.25$.

near field acoustics, and far-field acoustics of shock-containing plumes to uncover the physical mechanisms responsible for the generation of shock noise. A detailed discussion of the differences in the flow and the noise from convergent and convergent-divergent nozzles operated at supercritical nozzle pressure ratios (NPR) is provided in [2,7]. Our understanding of the main characteristics of broadband shock-associated noise, summarized above, resulted from these experimental investigations. The main ideas behind theoretical models are briefly summarized. Harper-Bourne and Fisher [1] first proposed that the passage of the turbulence through the shock cells and the ensuing interaction leads to the generation of broadband shock-associated noise. They viewed the sources as a phased array of monopoles located at the tips of the shock cells. This model leads to the presence of peaks at multiple higher harmonics of the fundamental frequency, if equal shock spacing is assumed. They also demonstrated that 1) the shock-cell spacing does not have a fixed value with their flow measurements, and 2) the higher harmonics were eliminated with a more realistic model for the shock spacing in their model. Tam and Tanna [7] chose to model the downstream-convecting turbulence as a random superposition of instability waves. A formal theory for the interaction of the turbulence structures with the shock cells was developed by Tam [11,12], which

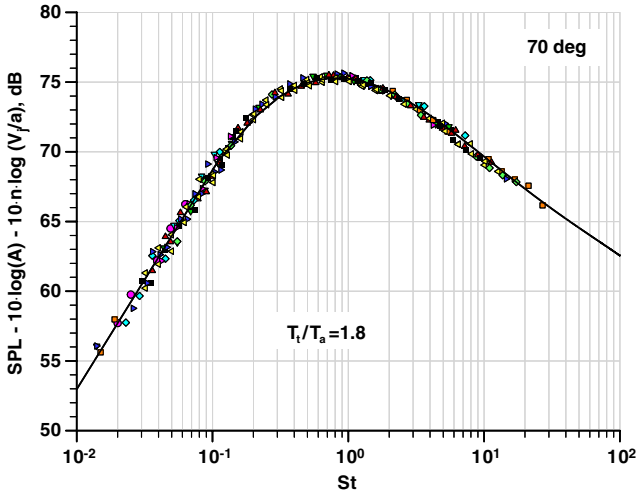

Fig. 3 Normalized spectra in symbols and curve fit, $T_t/T_a = 1.8$, and inlet angle = 70 deg.

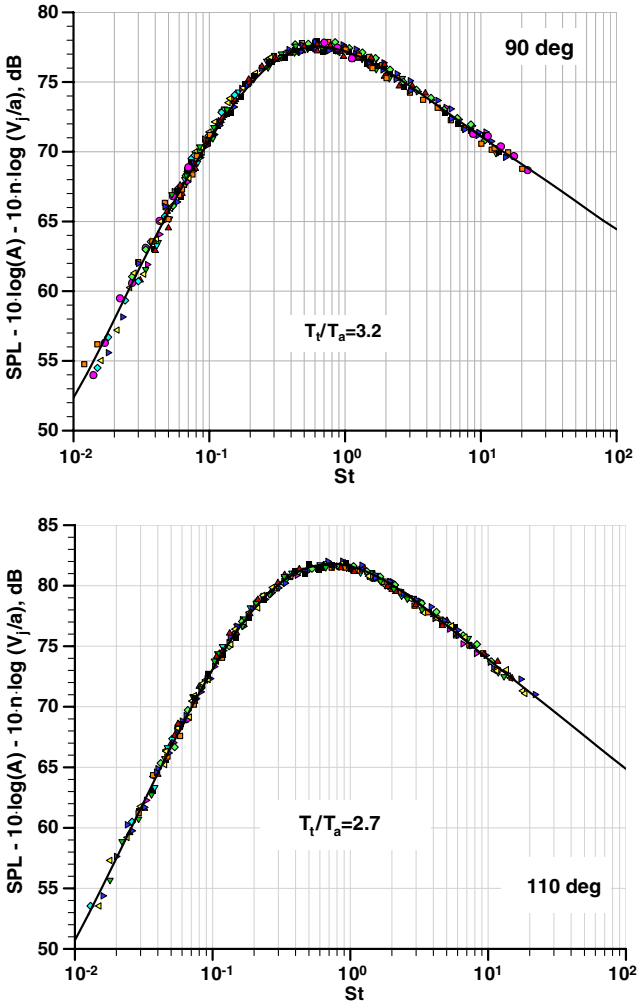

Fig. 4 Normalized spectra in symbols and curve fits. Top: $T_t/T_a = 3.2$, inlet angle = 90 deg; and bottom: $T_t/T_a = 2.7$, inlet angle = 110 deg.

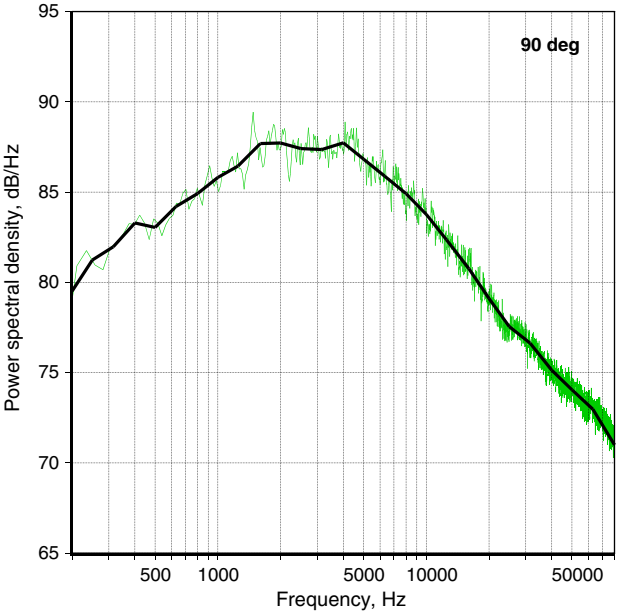

Fig. 5 Comparison of power spectral density, $M = 0.9$. Black: bandwidth-corrected one-third octave spectrum, and green: measured narrowband spectrum.

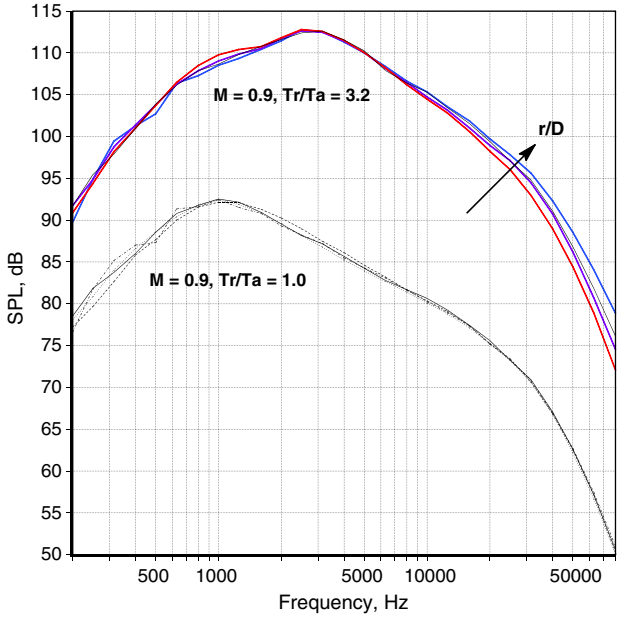

Fig. 6 Data normalized to 20 ft and standard-day conditions from measurements at different microphone distances: angle = 150 deg; $M = 0.9$, $T_t/T_a = 1.0$ and 3.2. Upper curves: red: $r = 10.59$ ft, violet: 16.59 ft, black: 22.59 ft, and blue: 30.59 ft.

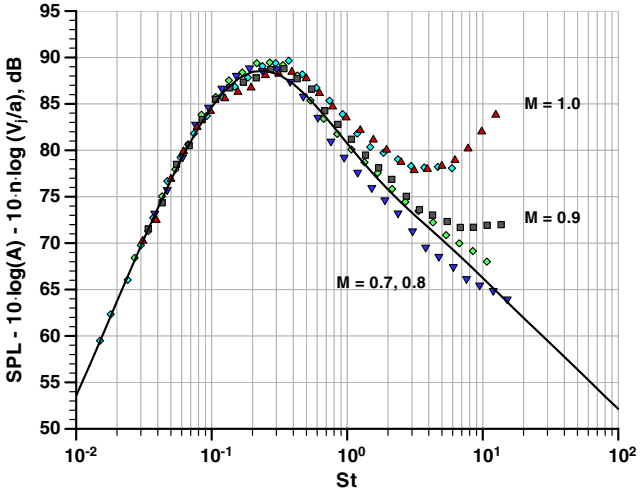

Fig. 7 Normalized spectra and curve fit $T_t/T_a = 3.2$, inlet angle= 145 deg. Spectra from $M = 0.9$ and $M = 1.0$ jet are not used in curve fit.

captured the experimentally observed characteristics very well. Thus, the physical mechanism is well explained by this theory.

One approach, wherein the noise from a convergent nozzle is compared with that from a CD nozzle at its design Mach number to identify the turbulent mixing noise, provides unambiguous results. However, it is not practical because one would have to design, build, and test numerous CD nozzles. Clearly, a reliable and practical method for identifying the turbulent mixing noise and broadband shock noise components from the measured total spectrum at any

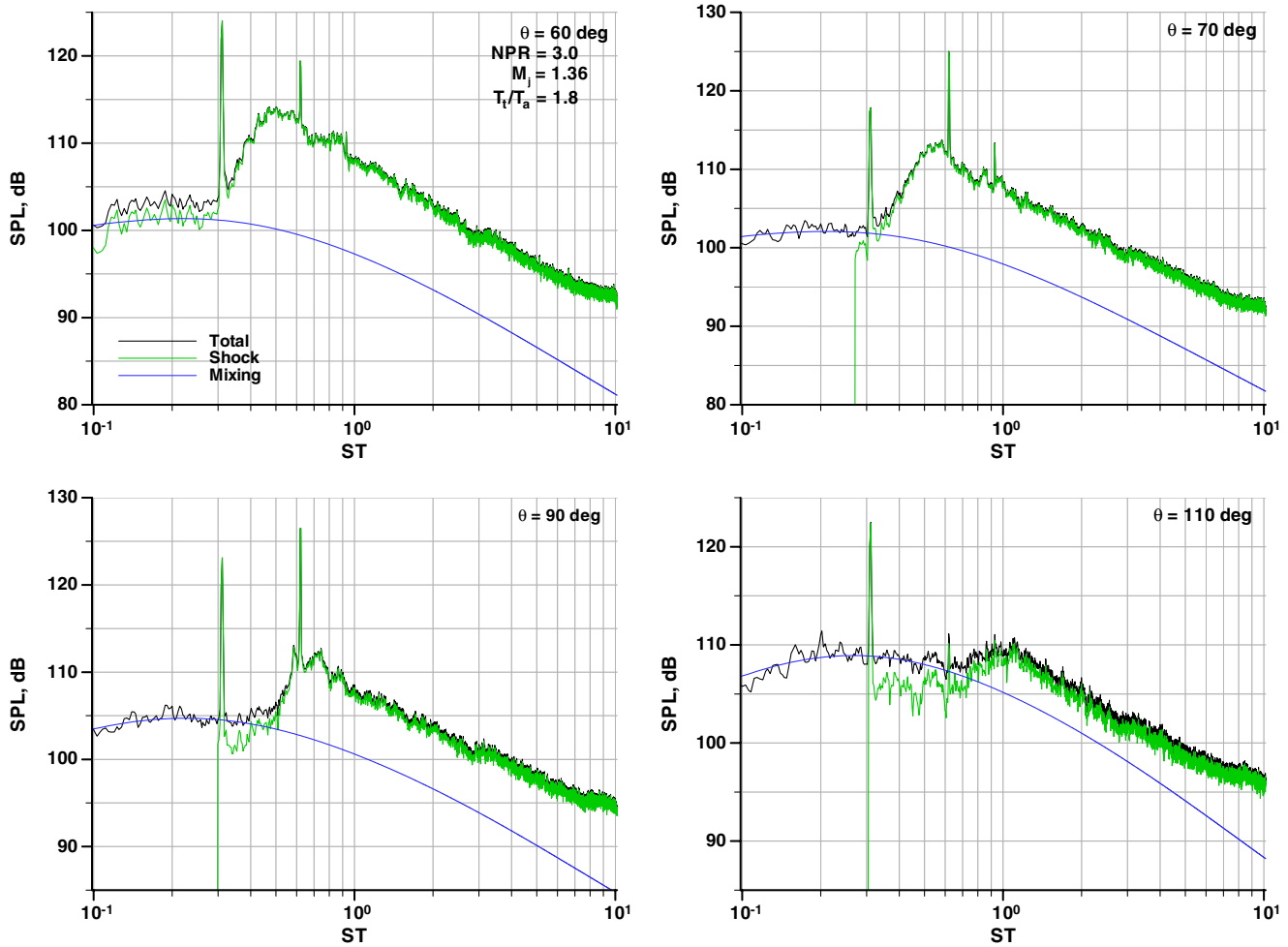

Fig. 8 Comparison of extracted mixing and shock-associated (broadband and screech tones) noise; $M = 1.36$, and $T_t/T_a = 1.8$. Black: total, blue: mixing noise, and green: shock noise.

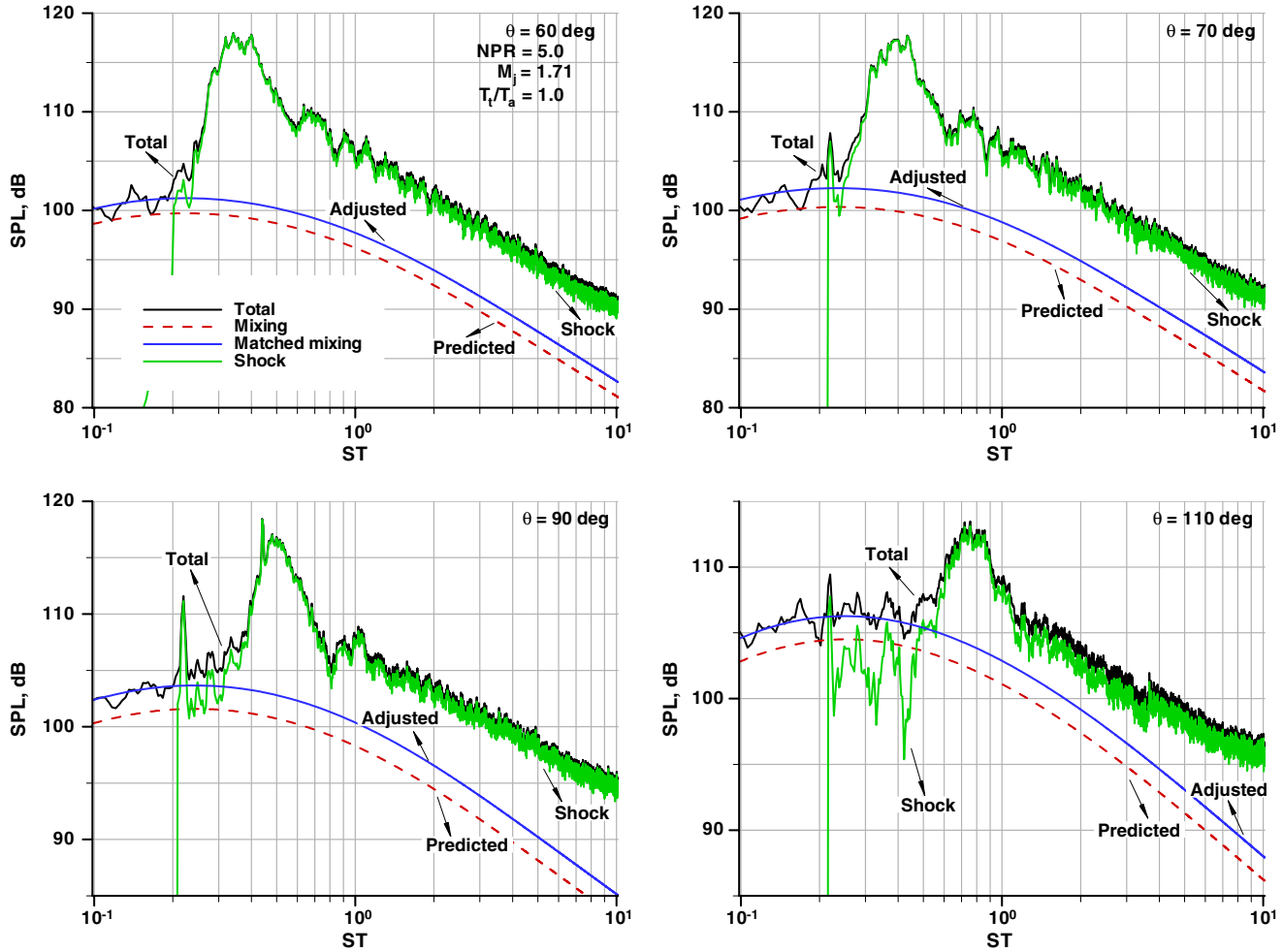

Fig. 9 Comparison of extracted mixing and broadband shock-associated noise; $M = 1.71$, and $T_t/T_a = 1.0$. Black: total, green: shock noise, blue: adjusted mixing noise, and dashed: predicted mixing noise.

angle is desirable. At the lower inlet angles, the noise at the higher frequencies has been attributed to the broadband shock component; the noise at the lower frequencies, to the left of the broadband shock peak, has been attributed to the mixing noise component. Moreover, the scaling relationships for broadband shock-associated noise have been established from the intensity or the overall sound pressure level (OASPL) of the entire spectrum, because of the lack of a simple method to separate the two components. The most commonly accepted relation for the intensity of shock noise is the proportionality with $(M_j^2 - M_d^2)^2$; the intensity is essentially dependent only on the nozzle pressure ratio and independent of the jet temperature and the observer angle [1]. In this expression, M_d is the design Mach number for a CD nozzle and is equal to unity for a convergent nozzle.

In this paper, we examine the characteristics with the analyses of new data. Further, the total measured spectra are first decomposed into the mixing and the broadband shock-associated components, and the characteristics of the shock component alone are investigated. The decomposition is made possible by a recently developed scaling methodology, an overview of which is provided in the next section. The database and the results are described in subsequent sections. Throughout this paper, we refer to the broadband shock component simply as the shock component.

II. Component Extraction

The approach for the extraction of the mixing and broadband shock components is the following. The measured spectra are normalized using new scaling laws for the turbulent mixing noise first. The scaled mixing spectrum at any angle is then subtracted from the total measured spectrum to obtain the broadband shock component.

Recently, Viswanathan [13,14] developed new scaling laws for the turbulent mixing noise, which produce excellent collapse of the spectra at different V_j/a [V_j is the jet velocity and a is the ambient speed of sound] but at fixed jet stagnation temperature ratio T_t/T_a. The new scaling laws also allow the identification of the two components of mixing noise and shock-associated noise from the total measured spectra, without any assumptions or subjectivity. This

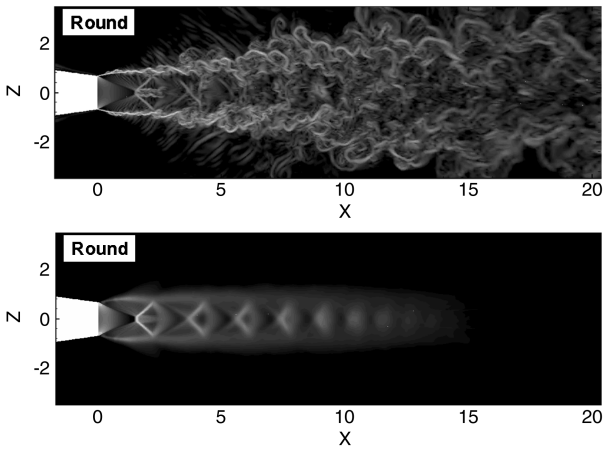

Fig. 10 Numerical schlieren: $M = 1.56$, and $T_t/T_a = 3.2$. Top: instantaneous density gradient, and bottom: time-averaged pressure gradient.

process is facilitated by the observation that the turbulent mixing noise is unaffected by the presence of shocks in the jet plume, as long as there are no strong screech tones, see section III. A. in Viswanathan [13]. Experimental evidence for this phenomenon was offered in figures 1 and 2 in [13] and in figures 12 and 14 in [15]. The basic philosophy behind the decomposition process is based on the following observations: the turbulent mixing noise generally scales with $(V_j/a)^n$, and the shock-associated noise scales with

$$\left[\sqrt{|M_j^2 - M_D^2|}\right]^m$$

In the classical theories $n = 8$ and $m = 4$. It has also been demonstrated by Viswanathan and Czech [16] that the scaling laws in which the primacy of the temperature ratio is recognized work equally well in correlating spectra from jets at constant static temperature (T_j/T_a) as well. The spectral characteristics for the turbulent mixing noise at any angle can be written as:

$$\text{SPL}\,(\theta, St) = F\left(\theta, St, \frac{T_t \text{ or } T_j}{T_a}\right)\left[\frac{V_j}{a}\right]^n, \quad n = n\left(\theta, \frac{T_t \text{ or } T_j}{T_a}\right) \tag{1}$$

The sound pressure level (SPL) per unit area (or area-normalized SPL) at an arbitrary fixed distance is given by the product of a spectrum function and the velocity ratio raised to the velocity exponent n. The spectrum function F and exponent n, at a particular angle and temperature ratio, are obtained from experimental measurements. When the parameter $[\text{SPL} - 10^*\text{Log}_{10}(A/A_{\text{ref}}) - 10^*n^*\text{Log}_{10}(V_j/a)]$ for one-third octave spectra or $[\text{SPL} - 10^*\text{Log}_{10}(A/A_{\text{ref}}) - 10^*n^*\text{Log}_{10}(V_j/a) - 10^*\text{Log}_{10}(D/V_j)]$ for narrowband spectra (acquired with constant bandwidth) are plotted against Strouhal number, a master spectral shape results for every angle and every temperature ratio. A is the nozzle exit area and A_{ref} is a reference area, which is taken to be one square inch here for convenience. This is the above spectrum function $F(\theta, St, T_t/T_a)$. The velocity exponent n has a unique value and is calculated from the measured overall sound pressure levels at each angle, from jets of different (V_j/a), but fixed jet static or stagnation temperature ratio.

The turbulent mixing noise for the supersonic cases is identified as follows. The lossless spectra from the subsonic jets at the selected temperature ratio are normalized, and the velocity exponents at all radiation angles are determined. The parameter $[\text{SPL} - 10^*\text{Log}_{10}(A/A_{\text{ref}}) - 10^*n^*\text{Log}_{10}(V_j/a)]$ is plotted on the y-axis for both the subsonic and supersonic Mach numbers. In the above relation, A is dimensional; one could express this area in terms of square inches, square feet or square meters. Depending on the chosen dimensional unit, the value of the spectral levels would move up or down by a scaling constant. For example, the noise per square foot would be higher than the noise per square inch by 21.58 dB $[10^*\text{Log}_{10}(144)]$. However, a consistent use of the same dimensional unit should result in the correct noise levels, regardless of the unit chosen. The dimensional area in square inches is used here. Sample spectra for $T_t/T_a = 3.2$ and at an inlet angle of 70 deg are shown in Fig. 1 for three subsonic Mach numbers and three supersonic Mach numbers. For the supersonic cases, the nozzle exit area is calculated using the fully expanded jet diameter. The fully expanded jet diameter for both convergent and CD nozzles for any jet Mach number can be calculated using the formula developed by Tam and Tanna [7].

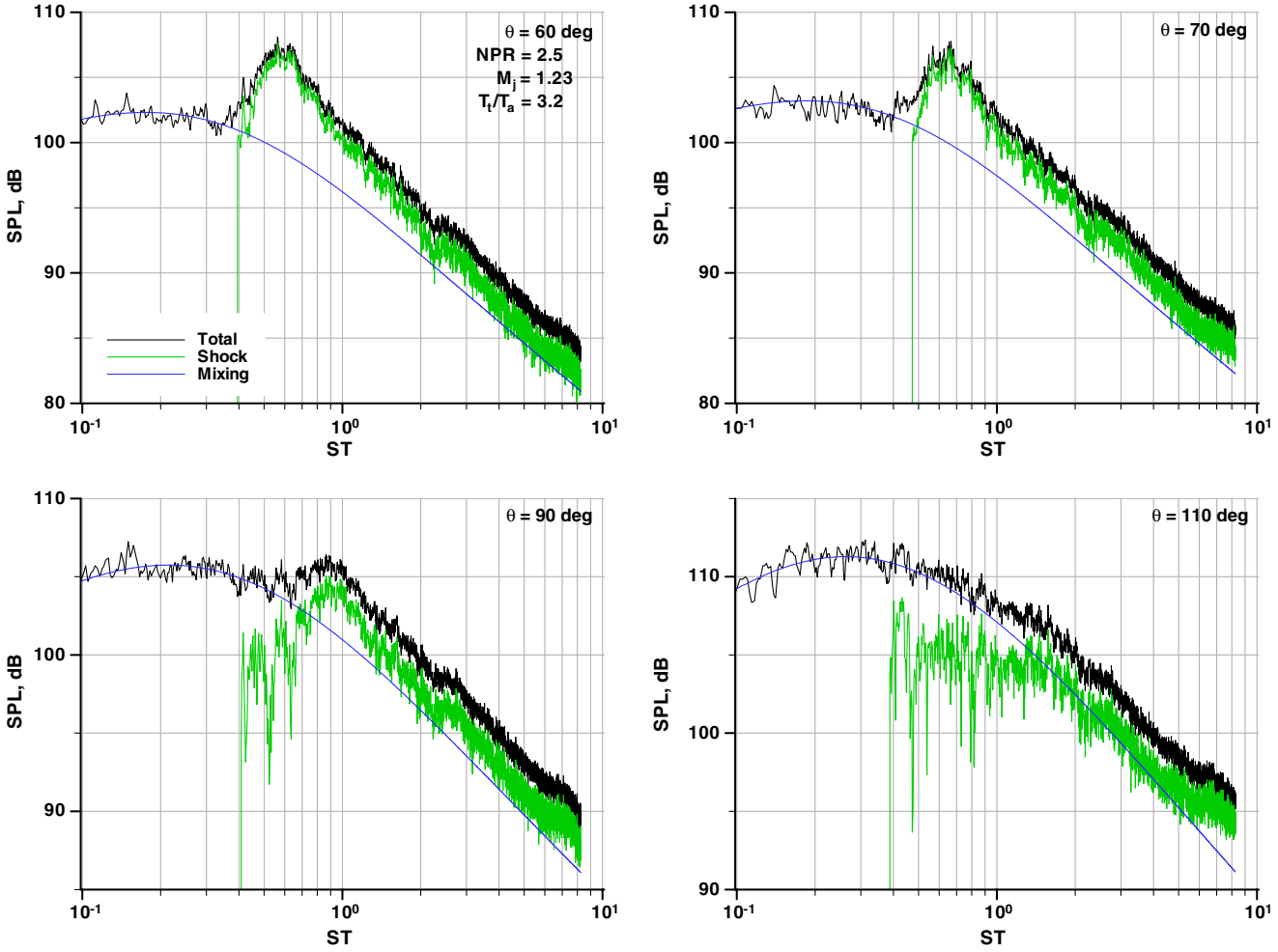

Fig. 11 Comparison of extracted mixing and broadband shock-associated noise; $M = 1.23$, and $T_t/T_a = 3.2$. Black: total, blue: mixing noise, and green: shock noise.

The data are corrected to a common (arbitrary) distance of 20 ft (6.096 m) from the center of the nozzle exit (coordinate system with origin at the center of the nozzle exit) and lossless or standard-day conditions: ambient temperature of 77°F (298°K) and relative humidity of 70%. The atmospheric attenuation coefficients are obtained from the method of Shields and Bass [17]. When lossless spectra are considered, the spectral levels just move up (or down) when the observer distance is reduced (or increased). Therefore, the choice of 20 ft has no special significance. The standard practice of converting the as-measured data to lossless form and then propagating the spectra to a common distance (of 20 ft) while accounting for the atmospheric absorption at standard-day conditions are adopted for general aircraft noise prediction. Implicit in this process is the assumption of linear propagation, with the sound pressure level obeying the $(1/r^2)$ dependence. The normalization process may be written as,

$$\mathrm{SPL}_{(r\ \mathrm{ft})} = \mathrm{SPL}_{\mathrm{measured}} - 10\mathrm{Log}_{10}\left(\frac{r}{R}\right)^2 + R[AA_{(\mathrm{test\ day})}] - r[AA_{(\mathrm{std\ day})}] \tag{2}$$

where R ft is the distance of the microphone from the origin of the coordinate system, AA are the atmospheric absorption coefficients (which are frequency dependent) per foot. The above equation

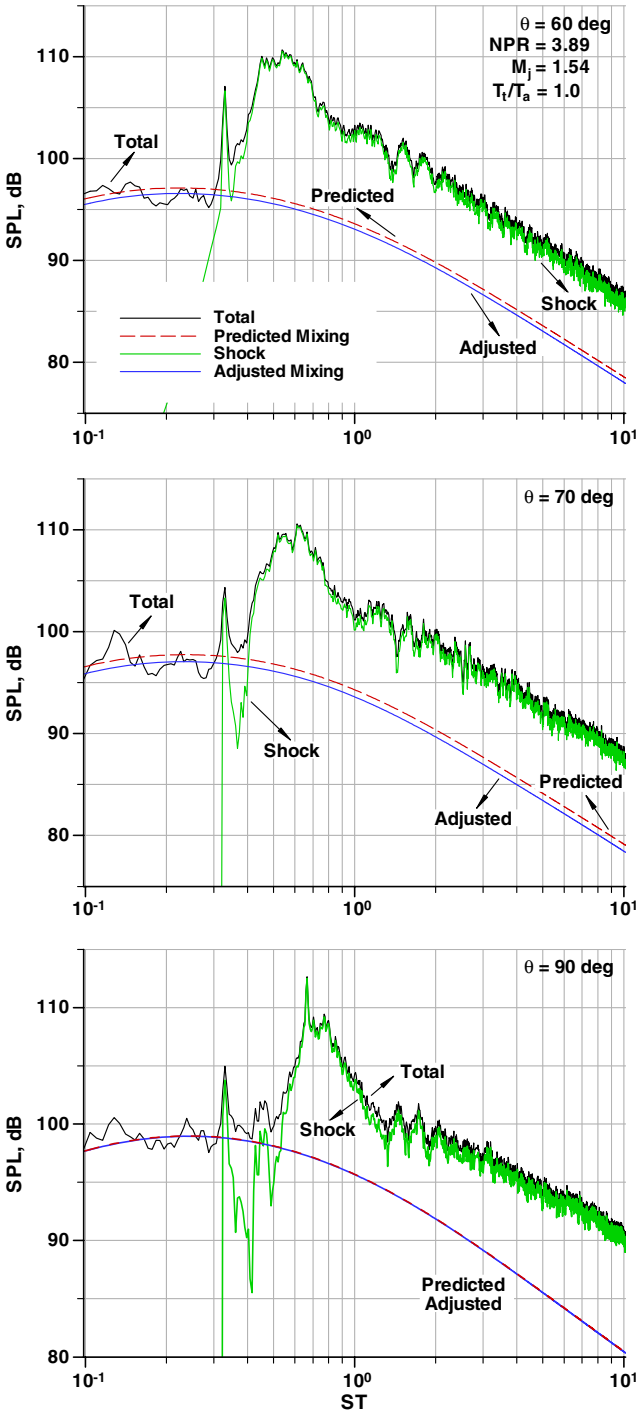

Fig. 12 Comparison of extracted mixing and shock-associated noise; $Mj = 1.54$, $Md = 1.76$, and $T_t/T_a = 1.0$. Black: total, green: shock noise, blue: adjusted mixing noise, and dashed line: predicted mixing noise.

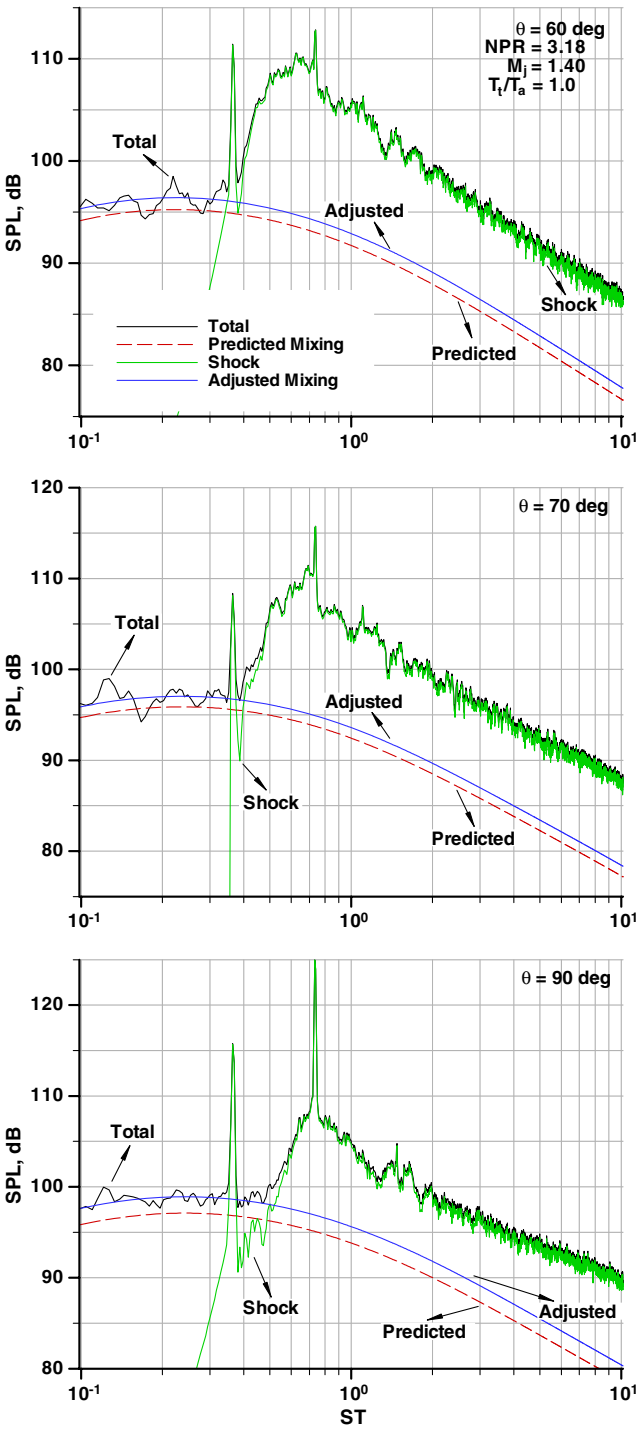

Fig. 13 Comparison of extracted mixing and shock-associated noise; $Mj = 1.4$, $Md = 1.56$, and $T_t/T_a = 1.0$. Black: total, green: shock noise, blue: adjusted mixing noise, and dashed line: predicted mixing noise.

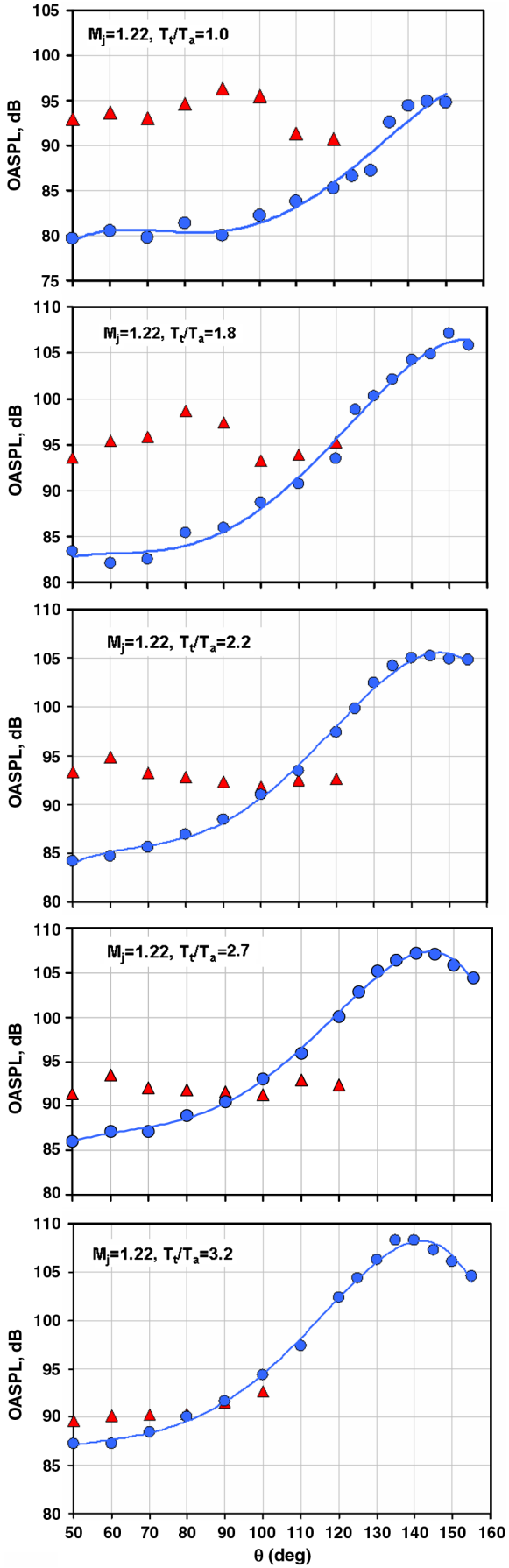

Fig. 14 Directivity of the mixing and shock components at different temperature ratios; $Mj = 1.22$. ▲: shock noise, and ●: mixing noise.

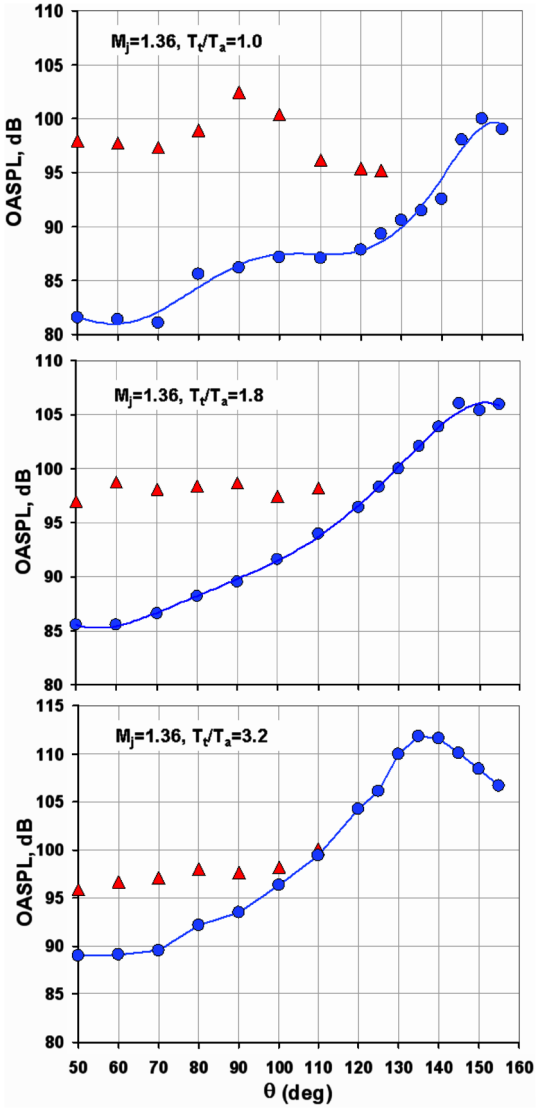

Fig. 15 Directivity of the mixing and shock components at different temperature ratios; $Mj = 1.36$. ▲: shock noise, and ●: mixing noise.

provides spectra corrected to standard-day conditions; for lossless data, the last term in this equation is omitted. The accuracy of the weather corrections and the suitability of the different proposed methods have been evaluated by Viswanathan [18]; it was shown that the method of Shields and Bass [17] was the best at the higher frequencies of interest in model-scale tests.

In Fig. 1, and in all the subsequent figures, lossless spectra are shown, unless otherwise stated. With the application of the method described above, there is excellent collapse of the subsonic mixing noise spectra (denoted by the symbols) over the entire frequency (Strouhal number) range. The spectra at the lower Mach numbers (not shown) extend the upper limit of the Strouhal number range, because of lower V_j. We further note that the spectra at the supersonic Mach numbers (denoted by lines) agree well with the subsonic ones at the lower frequencies. It is clear that the mixing noise component for the supersonic jets is given by the subsonic spectral shape denoted by the symbols. As noted in Viswanathan [13], the presence of strong screech tones could amplify the turbulent mixing noise; in such situations, it is necessary to adjust the spectral levels of the subsonic mixing noise by ∼1–∼2 dB to match the amplified mixing noise for the supersonic jets. The justification for this adjustment is provided in Section V.A. A simple logarithmic subtraction of the mixing noise spectrum from the total allows an unambiguous extraction of the shock-associated noise from the measured spectra. Several examples are shown in [13].

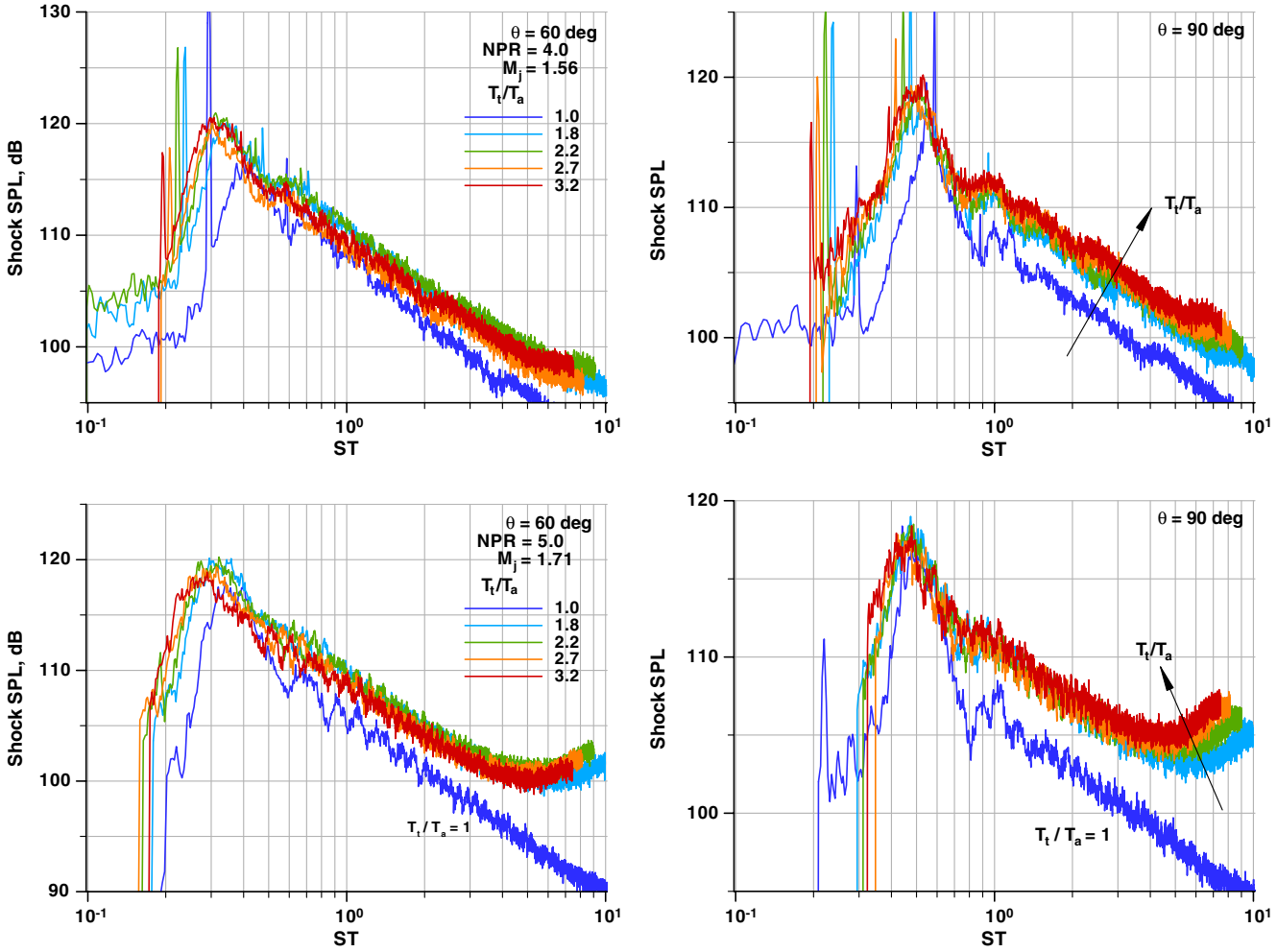

Fig. 16 Effect of jet temperature on shock component; top: $Mj = 1.56$, and bottom: $Mj = 1.71$.

III. Experimental Database

The description of the aeroacoustic database is provided in Viswanathan [13,14]. Detailed descriptions of the test facility, the jet simulator, the data acquisition, and reduction process, etc., may be found in Viswanathan [19,20]. For the sake of completeness, a brief overview is provided here. Brüel & Kjær quarter-inch Type 4939 microphones are used for free-field measurements. The microphones are set at normal incidence and without the protective grid, which yields a flat frequency response up to 100 kHz. Typically, several microphone arrays are used; these arrays were at a constant sideline distance of 15 ft (4.572 m) from the jet axis and on a polar arc of 25 ft (7.62 m). Very fine narrowband data with a bin spacing of 23.4 Hz up to a maximum frequency of 88,320 Hz are acquired and synthesized to produce one-third octave spectra, with a center band frequency range of 200 Hz to 80,000 Hz. The sampling rate is 196, 608/s; data are typically acquired for 10 s, which provides 239 averages. It was shown in Viswanathan [18,20] that data are highly repeatable, with the scatter within ± 0.25 dB for the same nozzle and for the same test conditions. In general, the scatter can be taken to be within $\pm \sim 0.5$ dB.

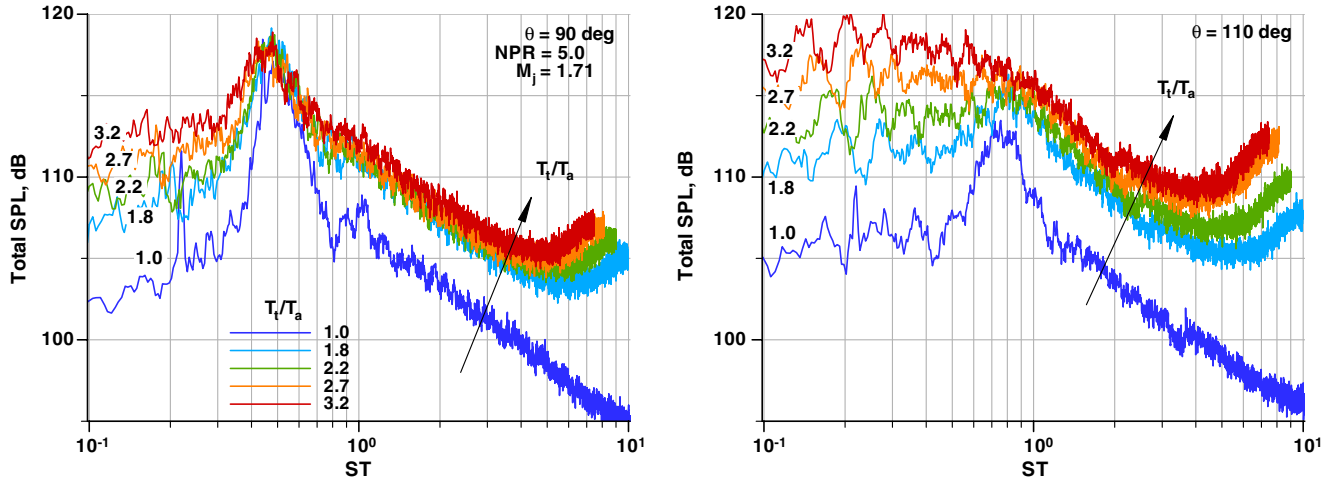

Fig. 17 Effect of jet temperature on total measured spectra; $Mj = 1.71$.

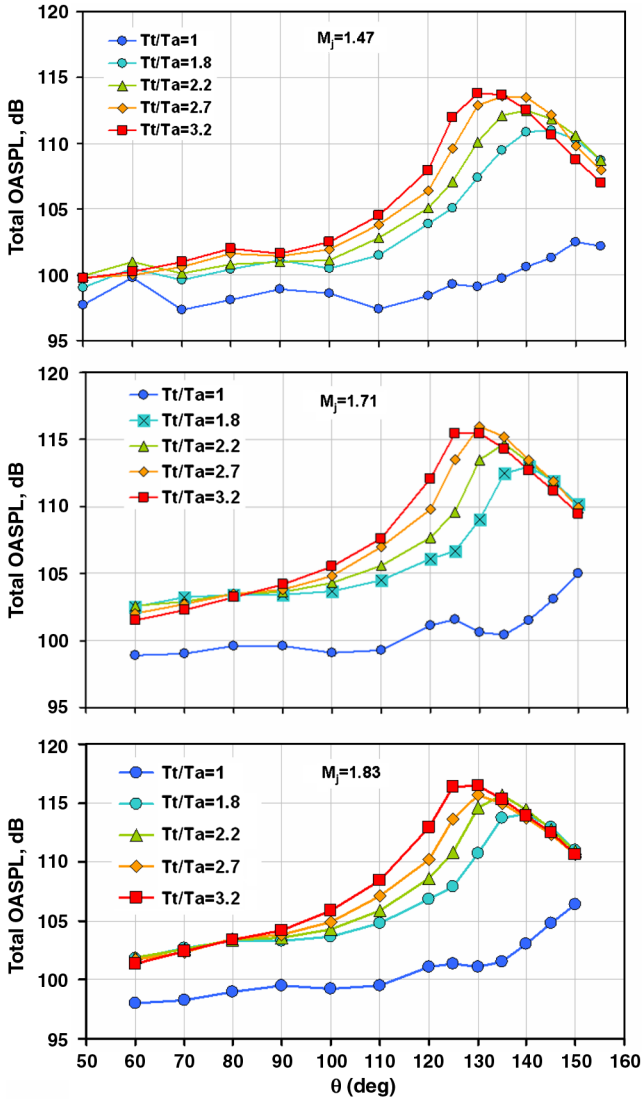

Fig. 18 Effect of jet temperature on total OASPL; $Mj = 1.47$, 1.71, and 1.83.

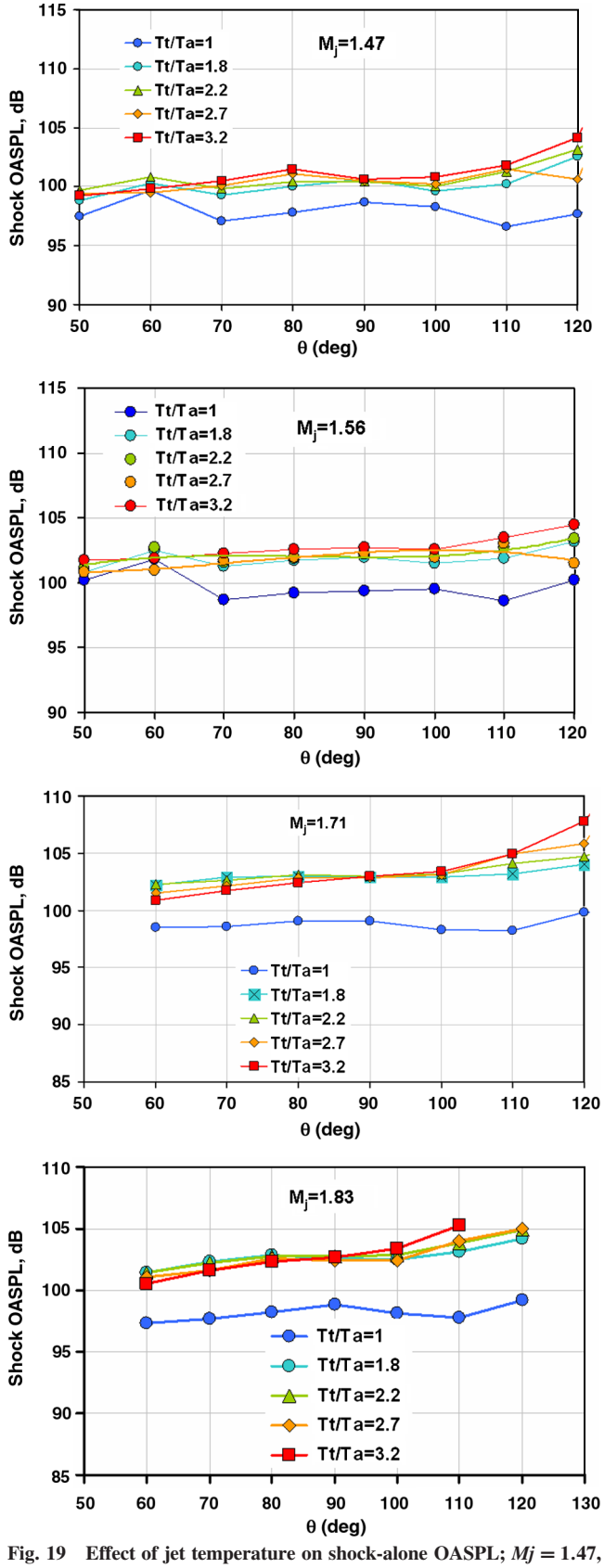

Fig. 19 Effect of jet temperature on shock-alone OASPL; $Mj = 1.47$, 1.56, 1.71, and 1.83.

Aeroacoustic data have been acquired at five stagnation temperature ratios (T_t/T_a) of 1.0, 1.8, 2.2, 2.7, and 3.2. The NPR are varied systematically to produce jets with Mach numbers of 0.4, 0.5, 0.6, 0.7, 0.8, 0.9, 1.0, 1.1, 1.24, 1.36, 1.47, 1.56, 1.71, and 1.83 at each jet temperature. The spectra from the subsonic jets are of course necessary to obtain the mixing noise component, as shown in Fig. 1. Conical nozzles (with $M_d = 1$) have been used for most cases and the broad range of supersonic Mach numbers yields shocks of varying strengths; in addition, two CD nozzles with design Mach numbers of 1.76 and 1.56 were tested.

IV. Methodology

A. Extraction of Spectra

The example shown in Fig. 1 contains one-third octave spectra. However, narrowband data are preferred for shock-associated noise because of the rich spectral details which get washed out when the narrowband spectra are synthesized to yield one-third octave spectra. The Strouhal scaling of broadband shock-associated noise was verified by Viswanathan [18]. The area-normalized spectra from unheated jets at two Mach numbers of 1.36 and 1.56 and from nozzles of three different diameters of 1.5 in., 2.45 in., and 3.46 in. are compared in figure 19 in Viswanathan [18]. There is excellent collapse over the entire Strouhal number range for the narrowband data as well. Figure 2 shows the collapsed narrowband spectra from two subsonic and two supersonic jets, for the same case of $T_t/T_a = 3.2$; this plot is comparable to Fig. 1, in which one-third octave spectra are shown. Again, the same consistent trends as seen in Fig. 1 are reproduced as far as the dominance of the two noise components at certain frequency regimes are concerned. Further, attention is drawn to the fact that the magnitude of the total spectrum

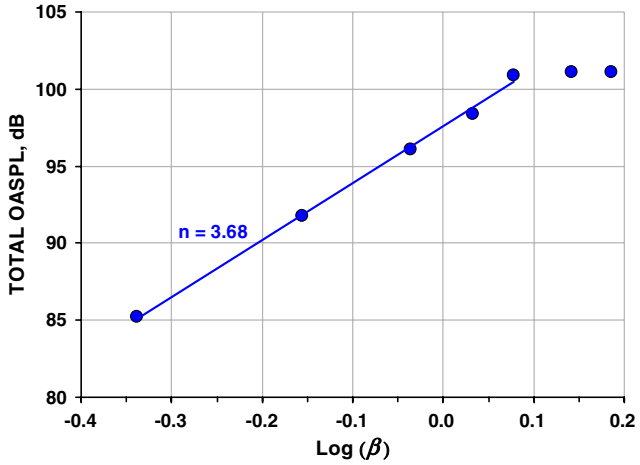

Fig. 20 Variation of total OASPL with log (β); $T_t/T_a = 1.0$, and angle = 120 deg. Symbols: data, line: least-squares fit through lowest five Mach numbers.

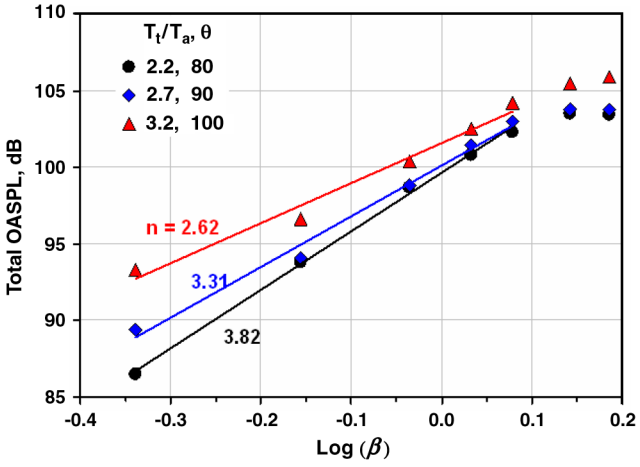

Fig. 21 Variation of total OASPL with log (β). Different jet stagnation temperature ratios and radiation angles as noted in inset.

for the $M_j = 1.24$ jet at the higher Strouhal numbers ($\geq \sim 2$) is only ~ 2 dB above the level for the mixing noise. As shown and discussed with one-third octave spectra in figure 10 in Viswanathan [13], the level of the extracted shock component is comparable to that of the mixing noise over a wide range of higher Strouhal numbers for moderately underexpanded heated jets. This observation directly contradicts the conventional belief that the shock component is dominant at the higher frequencies. At the higher jet Mach numbers for which the degree of underexpansion is severe, the shock noise clearly dominates at the higher frequencies, to the right of the spectral peak.

Here, we need a methodology for extracting the two noise components from narrowband spectra. This objective is accomplished as follows. The subsonic spectra from jets at different Mach numbers and V_j/a at every angle and at every temperature ratio have been collapsed with the experimentally obtained velocity exponent; the variation of the velocity exponent with radiation angle and temperature ratio is shown in figure 16 in Viswanathan [13]. A twelfth-order polynomial curve is fit through the data; several other orders for the curve fits were attempted and rejected. Figure 3 shows a sample curve fit at an inlet angle of 70 deg (all angles are measured from the jet inlet) for jets with $T_t/T_a = 1.8$; Fig. 4 shows two other examples one at an inlet angle of 90 deg for jets with $T_t/T_a = 3.2$, and another at an inlet angle of 110 deg for jets with $T_t/T_a = 2.7$. There is tight collapse of the one-third spectra in both plots; the spectral shapes are smooth at these and all other angles, thereby permitting accurate curve fits. Because of the well-behaved variation with Strouhal number, it is also justifiable to extrapolate the spectra beyond the measured frequency range as shown. However, caution must be

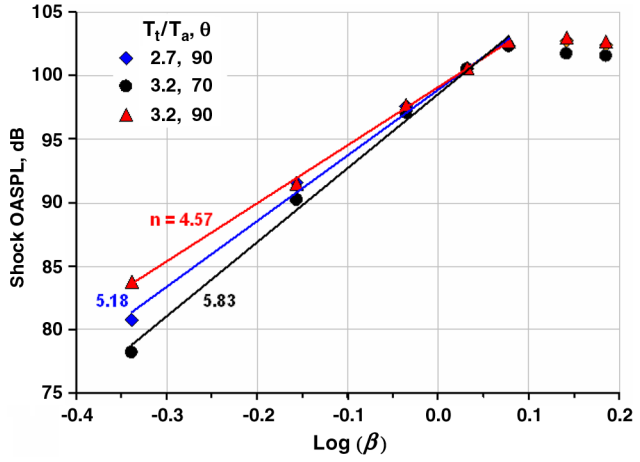

Fig. 23 Variation of shock OASPL with log (β). Different jet stagnation temperature ratios and radiation angles as noted in inset.

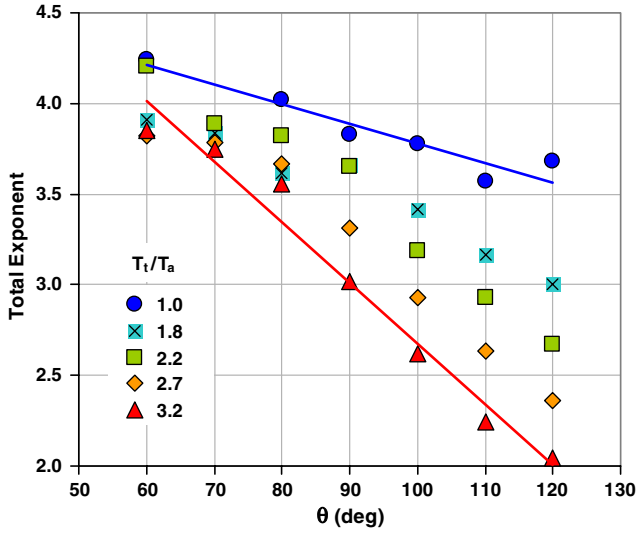

Fig. 22 Variation of the exponent for total OASPL with angle and temperature ratio.

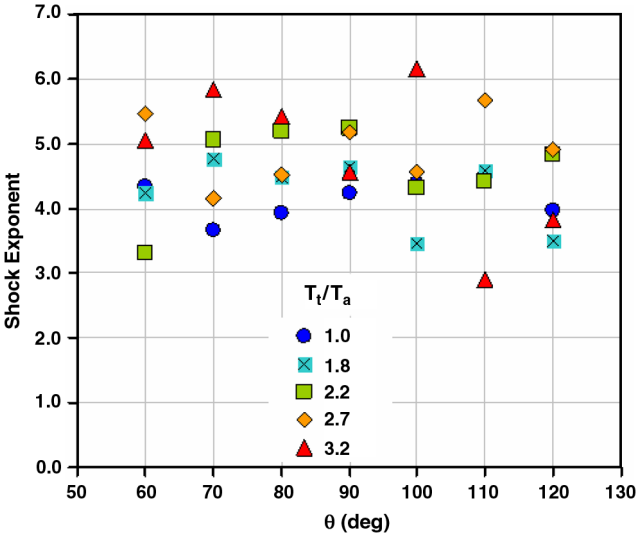

Fig. 24 Variation of the exponent for shock OASPL with angle and temperature ratio.

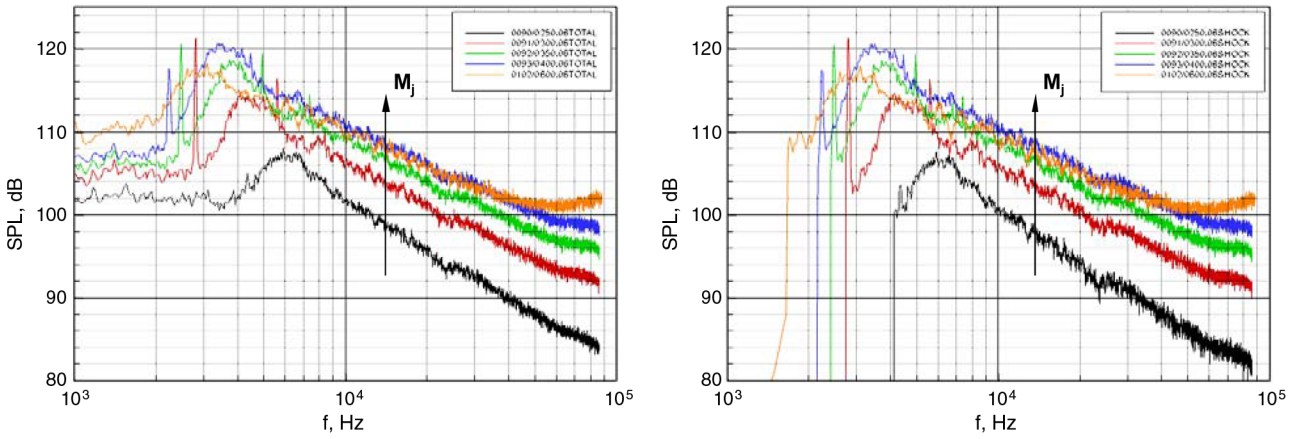

Fig. 25 Variation of a) total, and b) shock noise with Mach number; frequency on the x-axis; $T_t/T_a = 3.2$. Black: $M = 1.24$, red: $M = 1.37$, green: $M = 1.48$, blue: $M = 1.57$, and yellow: $M = 1.83$.

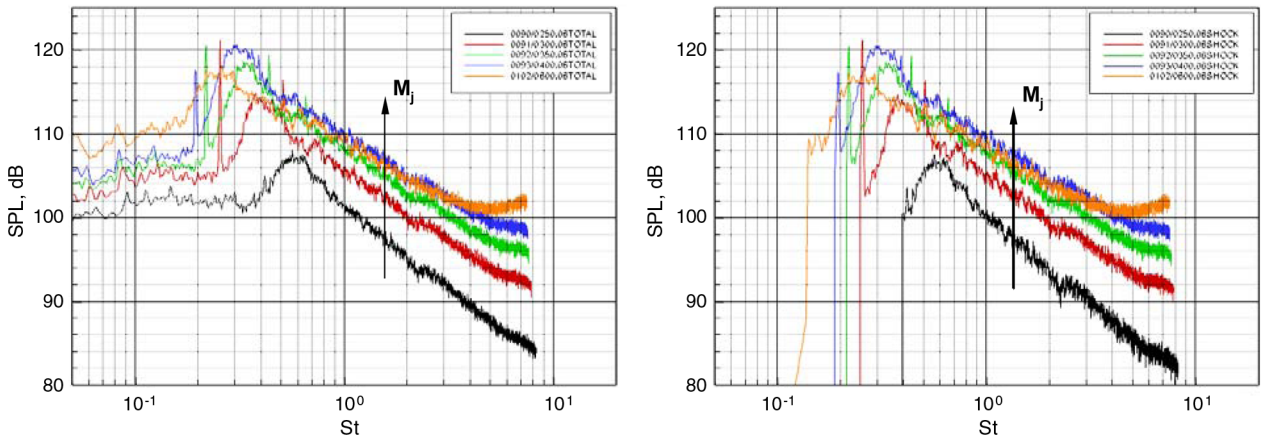

Fig. 26 Variation of a) total, and b) shock noise with Mach number; Strouhal number on the x-axis; $T_t/T_a = 3.2$. Black: $M = 1.24$, red: $M = 1.37$, green: $M = 1.48$, blue: $M = 1.57$, and yellow: $M = 1.83$.

exercised when extrapolating to very large values of Strouhal numbers. The curve fit can be used to predict the normalized one-third octave mixing noise spectrum at any angle and at any desired jet temperature ratio.

The various steps involved in the extraction of the narrowband spectra are enumerated:

1) Apply the normalization for the mixing noise $[\mathrm{SPL} - 10^{*}\mathrm{Log}_{10}(A/A_{\mathrm{ref}}) - 10^{*}n^{*}\mathrm{Log}_{10}(V_j/a) - 10^{*}\mathrm{Log}_{10}(D/V_j)]$ to the supersonic lossless power spectral density (dB/Hz).

2) Make an one-third octave prediction for mixing noise from curve fit.

3) Obtain a narrowband prediction for mixing noise by applying a bandwidth correction to the one-third spectrum; this is given by

$$\mathrm{SPL}_{\,\mathrm{narrowband}} = \mathrm{SPL}_{\mathrm{one\text{-}third}} - 10^{*}\mathrm{Log}_{10}(0.231^{*}f_c) \qquad (3)$$

where f_c is the center frequency of the one-third octave band in which the narrowband frequency of interest resides.

4) Adjust predicted narrowband spectra by $[-10^{*}\mathrm{Log}_{10}(D/V_j)]$.

5) To obtain shock spectrum, perform logarithmic subtraction of the normalized mixing noise from normalized total measured spectrum from supersonic jet.

6) Reverse the mixing noise scaling by adding $[10^{*}n^{*}\mathrm{Log}_{10}(V_j/a)]$ to the shock spectrum.

7) The resulting spectrum represents the as-measured shock component.

First we verify that the above approach is accurate in Fig. 5, with a comparison of the power spectral density (PSD) obtained from the bandwidth-corrected one-third octave spectrum with a measured narrowband PSD for a subsonic jet. Not surprisingly, the smooth black line lies in the middle of the narrowband spectrum with wiggles. There are obvious advantages in working with the one-third

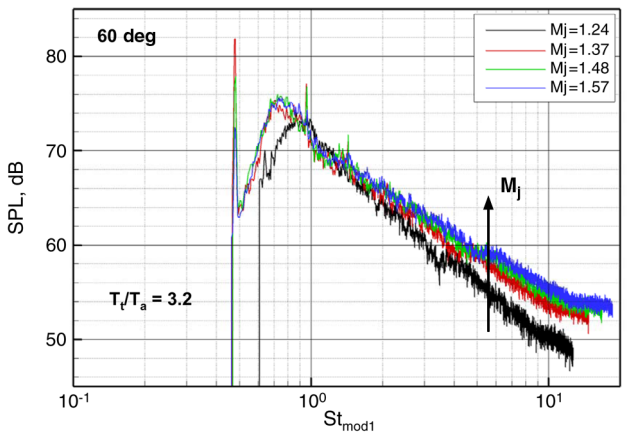

Fig. 27 Normalized shock noise at 60 deg at various Mach numbers; modified Strouhal number1 on the x-axis; $T_t/T_a = 3.2$. Black: $M = 1.24$, red: $M = 1.37$, green: $M = 1.48$, and blue: $M = 1.57$.

Table 1 Tabulation of the jet conditions and the observed linear or nonlinear propagation

NPR	T_t/T_a	V_j, ft/s	V_j/a	M_j	M_c	60 deg OASPL, dB	NL propagation
2.14	1.00	1110	0.99	1.10	0.69	84.1	No
5.00	1.00	1525	1.36	1.71	0.95	98.9	No
6.00	1.00	1590	1.42	1.83	0.99	98.0	No
2.14	1.80	1493	1.33	1.11	0.93	85.7	No
2.14	2.20	1653	1.47	1.11	1.03	85.0	No
2.14	2.70	1835	1.63	1.11	1.14	85.0	No
2.14	3.20	2002	1.78	1.12	1.25	85.4	No
2.50	3.14	2154	1.92	1.24	1.34	91.9	No
3.17	3.14	2383	2.12	1.41	1.48	98.9	Yes
3.50	3.14	2468	2.20	1.48	1.54	100.7	Yes
4.00	3.14	2575	2.29	1.57	1.60	102.4	Yes
3.00	3.51	2472	2.20	1.38	1.54	97.1	Yes
3.89	3.51	2705	2.41	1.56	1.69	102.2	Yes
4.50	3.51	2823	2.51	1.65	1.76	102.0	Yes
5.41	3.51	2959	2.63	1.78	1.84	101.3	Yes
5.00	1.80	2054	1.83	1.71	1.28	102.5	Yes
5.00	2.20	2276	2.03	1.71	1.42	102.6	Yes
5.00	2.70	2530	2.25	1.72	1.58	102.0	Yes
5.00	3.20	2767	2.46	1.72	1.72	101.5	Yes
6.00	1.80	2142	1.91	1.83	1.33	101.8	Yes
6.00	2.20	2374	2.11	1.83	1.48	101.9	Yes
6.00	2.70	2640	2.35	1.84	1.65	101.7	Yes
6.00	3.20	2888	2.57	1.84	1.80	101.4	Yes

spectra for the mixing noise component: the spectra are very smooth and the files are of manageable size. Consequently, the predicted PSD is also smooth, without the wiggles. As explained in Viswanathan [13], the presence of strong screech tones, especially for unheated jets, requires some adjustment to the level of the predicted mixing noise spectra.

B. Nonlinear Propagation Effects for Mixing Noise

Before the characteristics of the shock component are presented, the effects of nonlinear propagation on the spectra are briefly reviewed as they have a direct bearing on the results that are shown. The changes to the spectra due to nonlinear propagation for high-amplitude shock and blast waves are well established in the literature: the nonlinear distortion results in the steepening of the waveforms, a decrease in the zero crossings of the wave due to the coalescence of shock waves, and the transfer of energy from the spectral peak to both the low- and high-frequency portions of the spectra. Recently, Viswanathan [18,21] presented experimental evidence that indicates that the nonlinear propagation effects are not restricted to high-amplitude sound waves alone but are manifested even in subsonic heated jets encountered in model-scale tests in anechoic facilities. Concrete evidence was provided with spectra from four microphones located at distances of 10.59 ft, 16.59 ft, 22.59 ft, and 30.59 ft from the centerline of the nozzle exit plane.

A sample result, figure 10 from Viswanathan[18], is reproduced here as Fig. 6; the nozzle diameter for this case is 2.45 in. Normalized spectra from $M = 0.9$ jets with two temperature ratios of 1.0 and 3.2 are shown; the spectra from the four microphones have been corrected to a common distance of 20 ft (6.09 m), with the assumption of

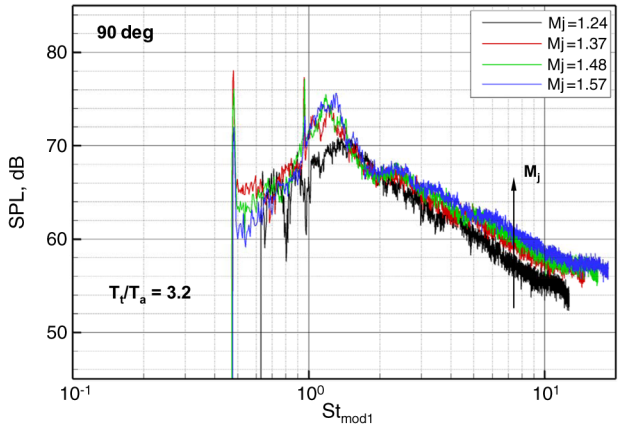

Fig. 28 Normalized shock noise at 90 deg at various Mach numbers; modified Strouhal number1 on the x-axis; $T_t/T_a = 3.2$. Black: $M = 1.24$, red: $M = 1.37$, green: $M = 1.48$, and blue: $M = 1.57$.

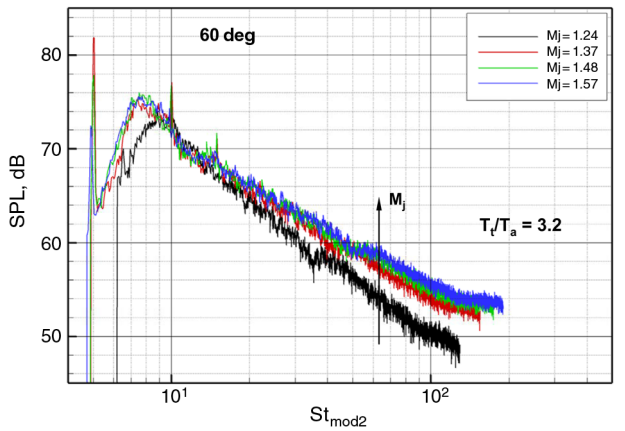

Fig. 29 Normalized shock noise at 60 deg at various Mach numbers; modified Strouhal number2 on the x-axis; $T_t/T_a = 3.2$. Black: $M = 1.24$, red: $M = 1.37$, green: $M = 1.48$, and blue: $M = 1.57$.

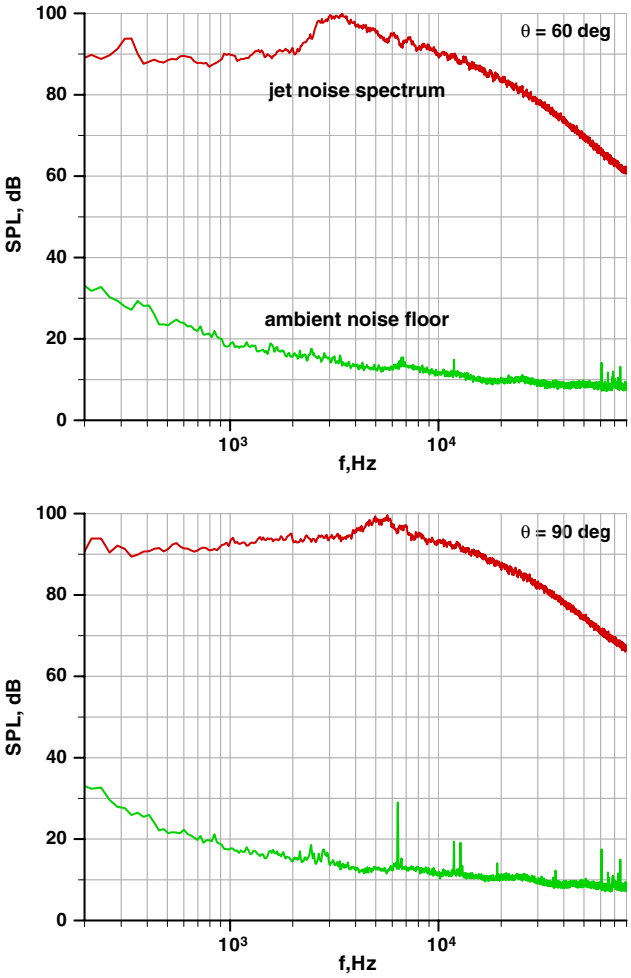

Fig. 30 Comparison of as-measured jet spectra and ambient noise floor; $M = 1.71$, and $T_t/T_a = 3.2$.

the sound pressure level obeying the $(1/r^2)$ dependence with distance. There is very good collapse of the spectra for the unheated jet with the assumption of linear propagation (lower set of curves). However, for the highly heated jet, nonlinear propagation effects, similar to those seen for the supersonic jets (see figure 9 in Viswanathan [18] for example) begin to appear. There is transfer of energy from the spectral peak to the higher frequencies; further, the levels at the higher frequencies increase with distance. Further analysis reveals that the convective Mach number (M_c), defined as the ratio of the convective velocity to the ambient speed of sound, just becomes supersonic for the $M = 0.9$ jet at a temperature ratio of 3.2. It has been established from experimental measurements that the average convective velocity is $\approx$70% of the mean jet velocity; this value has been assumed in the calculation of M_c. Viswanathan [14,18,21] proposed and provided experimental evidence that the convective Mach number is the most reliable indicator of the effects associated with the onset of nonlinear propagation in jet noise; see section III.C [18] and section IV.C [14]. It is also established in Viswanathan [14] that the angular range in which these effects are observed is $\geq \sim 130$ deg for heated subsonic jets with a maximum stagnation temperature ratio of 3.2.

Now, the jet velocities are much higher for the supersonic heated jets considered here. In the curve fits for the turbulent mixing noise, there is good collapse of the spectra from jets with subsonic M_c. However, the levels at the higher frequencies are a function of distance as seen in Fig. 6 for the convectively supersonic jets. There have been some attempts in the past to predict the levels as a function of distance; see Saxena et al. [22], for example. Therefore, only the spectra from jets with subsonic M_c have been used to develop the curve fits. A sample case, which illustrates this problem is presented in Fig. 7; the spectra correspond to those from heated jets with $T_t/T_a = 3.2$ at an aft angle of 145 deg. There is very good collapse of the spectra at the spectral peak and at the lower frequencies to the left of the peak. Note that there is good collapse of the spectra for the $M = 1.0$ jet from nozzles of two different diameters of 1.5 in. and 3.46 in. However, there are drastic differences at the higher frequencies, especially for the $M = 0.9$ and $M = 1.0$ jets. For instance, the spectral level for the $M = 1.0$ jet is $\sim$19 dB higher than that for the subsonic jets at a Strouhal of $\sim$12. It should be clearly recognized that this elevated level is still part of the turbulent mixing noise; for a supersonic jet, when we subtract the mixing noise based on the subsonic curve fit, the difference at the higher frequencies will be incorrectly assigned to the shock component. However, it should be kept in mind that this trend is not the actual case; the effects due to nonlinear propagation serve to muddle the separation process at the aft angles. For this reason, we restrict our analyses to a maximum angle of 120 deg; further, the mixing noise component is the dominant source in the peak radiation sector.

V. Results and Discussion

A. Separated Components

The application of the separation methodology is illustrated for a few sample cases, first with the spectra for under-expanded jets obtained with the convergent nozzles. Figure 8 shows the total measured spectra and the extracted components at four radiation angles; the jet conditions are $M_j = 1.36$ and $T_t/T_a = 1.8$. The PSD parameter $[\mathrm{SPL} - 10^*\mathrm{Log}_{10}(A/A_{\mathrm{ref}}) - 10^*\mathrm{Log}_{10}(D/V_j)]$ dB/St is plotted on the y-axis of all the narrowband spectral plots. Because of limited space in these plots, this quantity is simply denoted as SPL.

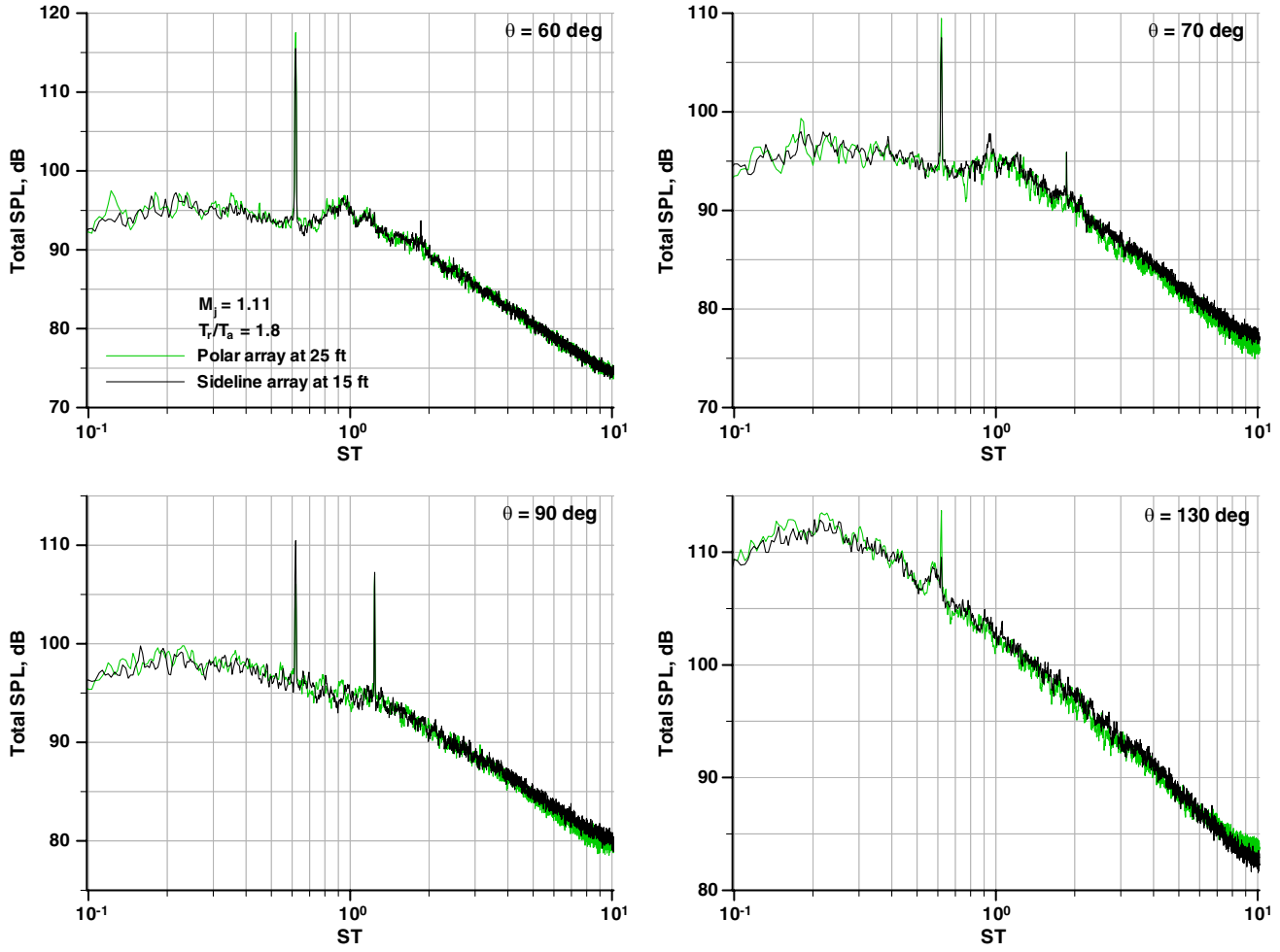

Fig. 31 Comparison of spectra from microphones at different locations normalized to fixed distance; $M = 1.1$, and $T_t/T_a = 1.8$. Green: 25-ft polar, and black: 15-ft constant sideline.

In general, it is necessary to adjust the level of the predicted mixing noise by ∼1 to ∼2 dB at each angle to match the measured spectrum at the lower frequencies (see third paragraph in this section). There is a strong screech tone, with higher harmonics at the lower polar angles. For this case, the mixing noise component is dominant only at the lower frequencies, with the shock noise clearly dominant at the higher frequencies. As we move aft, the importance of the mixing noise increases, typically for inlet angles ≥ ∼120 deg.

How accurate are the predictions for the supersonic jets? Figure 9 shows a comparable plot for an unheated jet at a higher Mach number of 1.71. In this figure, both the predicted spectra for the mixing noise (denoted by the dashed lines) and the adjusted spectra are shown. As seen, the adjustment is ∼2 dB. For this case, the shock component is the dominant source even at 110 deg because of the lower levels for the mixing noise. Attention is drawn to an interesting feature in the spectra: the strong screech tones have completely disappeared even though the Mach number for this unheated jet is much higher than the case shown in Fig. 8. This cessation of screech can be attributed to the formation of a Mach disk for this highly underexpanded jet. No optical observations or numerical simulations are available. However, sample results from a large eddy simulation for a $M_j = 1.56$ and $T_t/T_a = 3.2$ jet is reproduced from [23] as Fig. 10. It is clear that there is a Mach disk, with subsonic flow and an internal shear layer downstream of the Mach disk. It stands to reason that Mach disks will form for the much higher Mach numbers of 1.71 and 1.83. A third sample case is shown for a jet with $M_j = 1.23$ and $T_t/T_a = 3.2$ in Fig. 11. For this highly heated jet at a lower Mach number, the balance between the two components is very different; the levels are comparable at the higher frequencies even at the lower polar angles.

As noted in Viswanathan [14], it is not correct to think that the shock component is always the dominant source at the lower radiation angles.

Attention is drawn to another aspect of the scaling methodology and the prediction of the turbulent mixing noise from supersonic jets. The scaling laws, derived from subsonic spectra, are used to predict the mixing noise from jets with as high a Mach number as 1.83. The velocities for the $M_j = 1.83$ jets are ∼56% higher than the values for the $M_j = 1.0$ jet at the same jet total temperature. It is interesting that the scaled levels from the subsonic spectra are within ∼2 dB even for the $M_j = 1.83$ jets. This close agreement attests to the accuracy of the scaling laws and the robustness of the methodology. The justification for the adjustment is the following: experimental measurements with convergent and CD nozzles operated at the design Mach number of the CD nozzle have shown that the spectra at the lower frequencies are identical for both the nozzles. That is, the turbulent mixing noise component accounts for all the energy at these frequencies. Further, the consequence of not adjusting the level on the extracted shock component is illustrated in Fig. 8 at 60 deg, which shows the predicted mixing noise spectrum from the scaling laws. Because the predicted smooth line does not go through the wiggles in the total measured spectrum, the shock component exhibits wiggles and does not drop off sharply. Note that the predicted mixing level requires no adjustment when the degree of mismatch from the design Mach number is not large, as seen in Figs. 1 and 2 for the $M_j = 1.24$ case.

Next we consider overexpanded jets obtained with the CD nozzles. Figure 12 shows the separated components for an unheated jet with $M_j = 1.54$ and $M_d = 1.76$. The directly predicted mixing

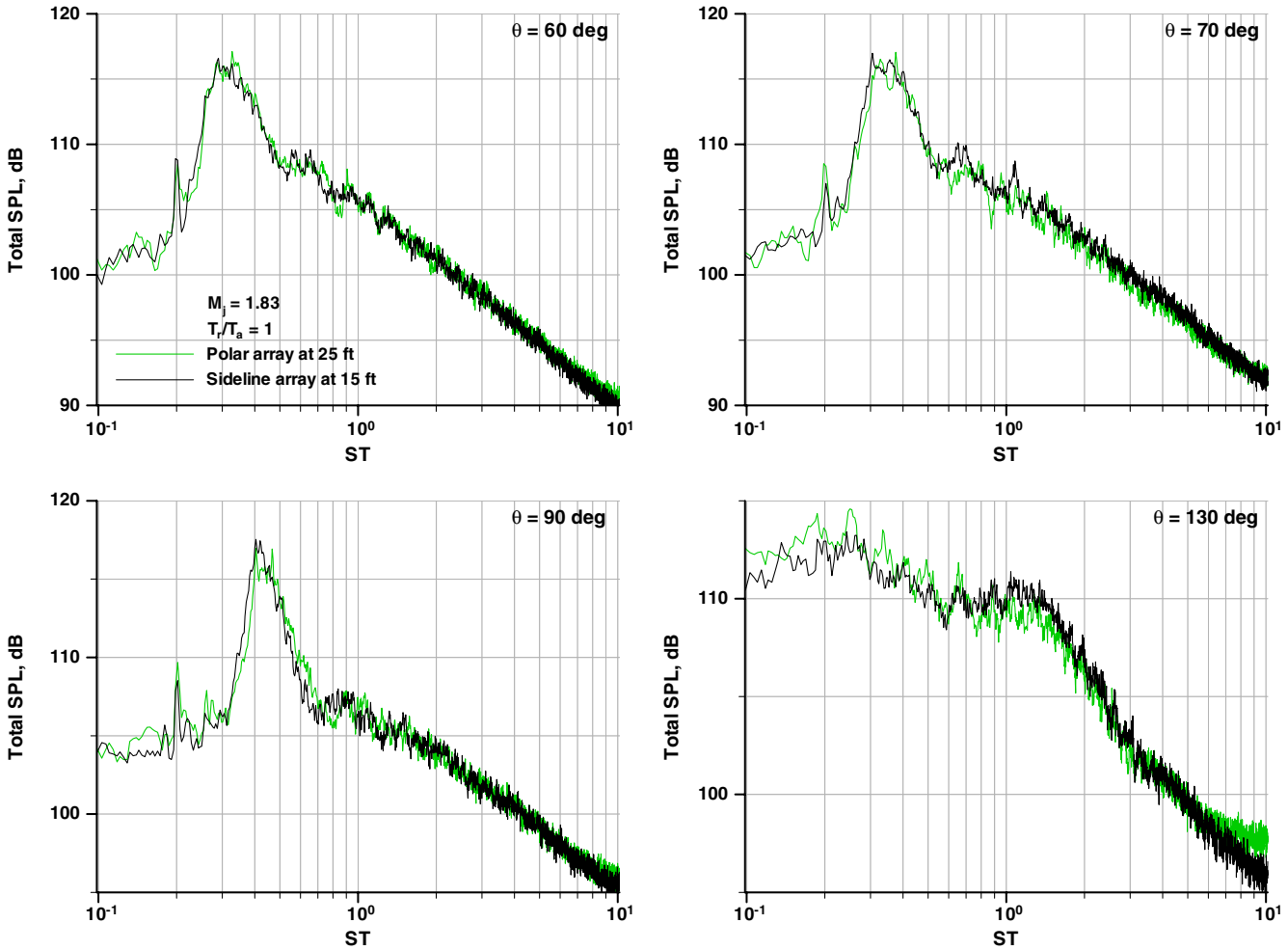

Fig. 32 Comparison of spectra from microphones at different locations normalized to fixed distance; $M = 1.83$, and $T_t/T_a = 1.0$. Green: 25-ft polar, and black: 15-ft constant sideline.

noise from the scaling laws and the adjusted mixing noise spectra are shown, in addition to the shock component. For this case, the adjustment is less than 1 dB at 60 deg and 70 deg; at 90 deg the predicted and adjusted levels are almost identical as the two curves virtually coincide. Figure 13 shows another example with $M_j = 1.4$ and $M_d = 1.56$. The magnitude of the adjustment is ~2 dB for this case. For both these unheated jets, the shock component is clearly dominant at the higher Strouhal numbers to the right of the broadband shock peak.

The experiments at NASA Langley Research Center by Seiner and Norum [3] showed that the low-frequency portions of the spectra from underexpanded and overexpanded jets at the same M_j are almost identical; see figure 14 in Tam et al. [15]. This figure shows spectral comparisons at $M_j = 1.37$ with $M_d = 1.0$ and 1.5 and at $M_j = 1.8$ with $M_d = 1.5$ and 2.0. This is precisely the frequency regime in which the mixing noise is the dominant component; that is, the mixing noise levels are unaltered by the presence of shocks, either due to overexpansion or underexpansion. It should be clear from the examples shown here in Figs. 8, 9, and 11–13 that the methodology developed here is equally applicable for spectra obtained with convergent and CD nozzles.

Now we examine the relative importance of the two components at various operating conditions. Figure 14 shows the directivities of the two components for an $M_j = 1.22$ jet at the five temperature ratios. For the unheated jet, the shock component is clearly dominant at the lower polar angles, with the levels being higher by ~12 dB. In the aft directions, the mixing noise is dominant. As the jet is progressively heated, the mixing noise levels increase monotonically and the difference in levels between the shock and mixing components decreases. At the highest temperature ration of 3.2, both the components have comparable levels at this jet Mach number. Figure 15 shows another example, but at a higher Mach number of 1.36. The trends are similar to those seen for $M_j = 1.22$. However, the shock component has higher absolute levels, as expected. Another notable feature in the directivity of the shock component is the following: the levels vary only slightly with radiation angle. The slightly elevated levels at some angles for the lower temperature jets ($T_t/T_a = 1.0$ and 1.8) are caused by screech tones. For the higher temperature jets, the shock component is omnidirectional in character; this result is consistent with past observations.

B. Effect of Jet Temperature on Shock Noise

The effects of increasing the jet temperature on the shock component for jets with fixed M_j are examined with sample results for two Mach numbers of 1.56 and 1.71 in Fig. 16. Note that the screech tones are absent for the heated jets for $M_j = 1.71$, thereby permitting clear interpretation of the data. The most striking trends from the spectra are the following: 1) there is good collapse of the spectra from the four heated jets at both Mach numbers and both angles, and 2) the spectral levels for the heated jets are higher than those of the unheated jets. Similar trends are observed at all the lower polar angles (not shown). Further, the screech tone frequency decreases progressively as the temperature is increased for $M_j = 1.56$. This decrease in tone frequency further confirms Tam's formula [[11,12]] for the prediction of the screech frequency. For the sake of completeness, the measured total spectra at two angles of 90 deg and 110 deg for the $M_j = 1.71$ jet are shown in Fig. 17. There is a marked difference in

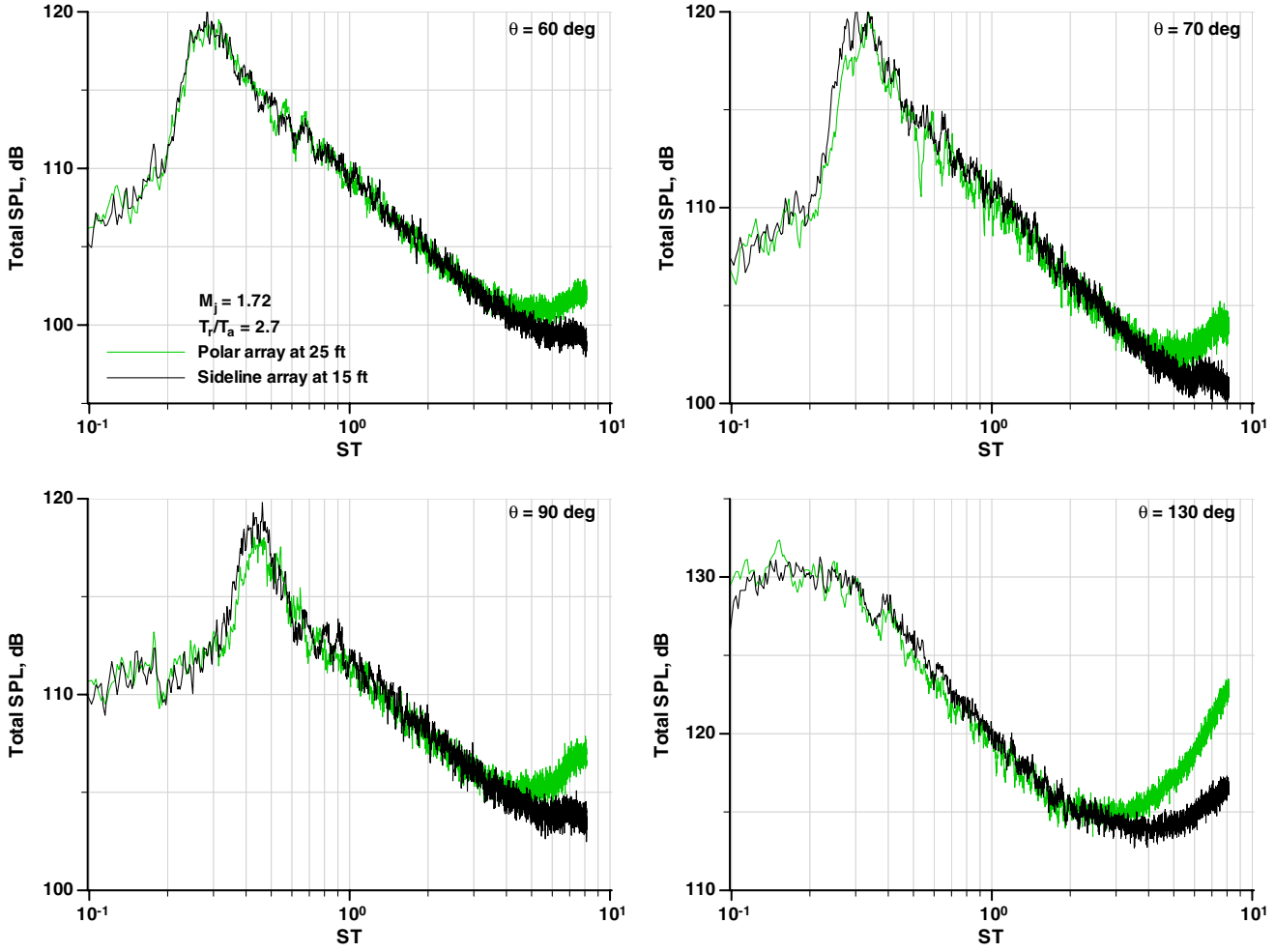

Fig. 33 Comparison of spectra from microphones at different locations normalized to fixed distance; $M = 1.72$, and $T_t/T_a = 2.7$. Green: 25-ft polar, and black: 15-ft constant sideline.

that there is a progressive increase in levels in the low-frequency portion of the measured spectra due to heating, clearly associated with the dominance of the mixing noise component at these frequencies. In Fig. 16, this part of the spectrum for all the cases has been removed in the extraction process resulting in good collapse of the shock components.

A better appreciation of the effect of jet temperature is obtained through the examination of the variations of the OASPL. Figure 18 shows the directivity of the total noise for three different jet Mach numbers of 1.47, 1.71, and 1.83, respectively. The curves are relatively flat at the lower polar angles, but the levels increase steeply with angle and jet temperature in the aft directions. The mixing noise component becomes dominant in the aft quadrant. Figure 19 shows the directivity of the shock-alone OASPL for the four Mach numbers of 1.47, 1.56, 1.71, and 1.83. First of all, the effect of jet temperature is more clearly observed when the mixing noise is removed. Secondly, there is an obvious increase in the shock noise levels with heating; however, once the jet is heated to say $T_t/T_a = 1.8$, the OASPL remains unchanged with further increases in temperature. For the higher Mach numbers of 1.71 and 1.83, the magnitude of the increase in OASPL is ~3 dB–~4 dB at all the lower polar angles. The directivity curves are flat for all temperatures, highlighting the omni-directional characteristic of the radiation of broadband shock-associated noise. The results presented here, in terms of spectral comparisons and the directivities of the OASPL, indicate a clear effect of the jet temperature on shock noise. This effect has never been reported in prior studies. The saturation of the OASPL with jet temperature is puzzling; the physical reasons for this phenomenon are unknown at this time.

C. Scaling Relation for Shock Noise

The variation of the OASPL with radiation angle and jet temperature is examined, both for the total noise (shock and mixing components) first, and then for the shock component alone obtained through subtraction of the mixing noise.

1. *Total Noise*

As already noted, the intensity is thought to depend on $(M_j^2 - M_a^2)^2$, also usually referred to as β^4, where β is given by

$$\sqrt{|M_j^2 - M_D^2|}$$

and independent of the jet temperature and the observer angle, as per conventional belief. In the computation of the OASPL, no effort has been made to remove the screech tones, as these are part of the as-measured spectra. However, the effects of the formation of the Mach disk for the extremely high underexpanded jets need to be considered. In addition to the elimination of the strong screech tones noted in Fig. 9, the data indicate that there is a saturation of the noise levels. Because of this, the OASPL at the highest two Mach numbers of 1.71 and 1.83 are not included in the estimation of the power law for the OASPL. For the sake of information, the OASPLs at these higher Mach numbers are also included in the following figures.

The computed OASPLs for the total measured noise are plotted against $[\mathrm{Log}_{10}(\beta)]$ and a least-squares fit is drawn through the data points. The value of the exponent that collapses the OASPL is given by the slope divided by ten. Figure 20 shows a typical variation for jets with $T_t/T_a = 1.0$ at an angle of 120 deg. The curve fit with a

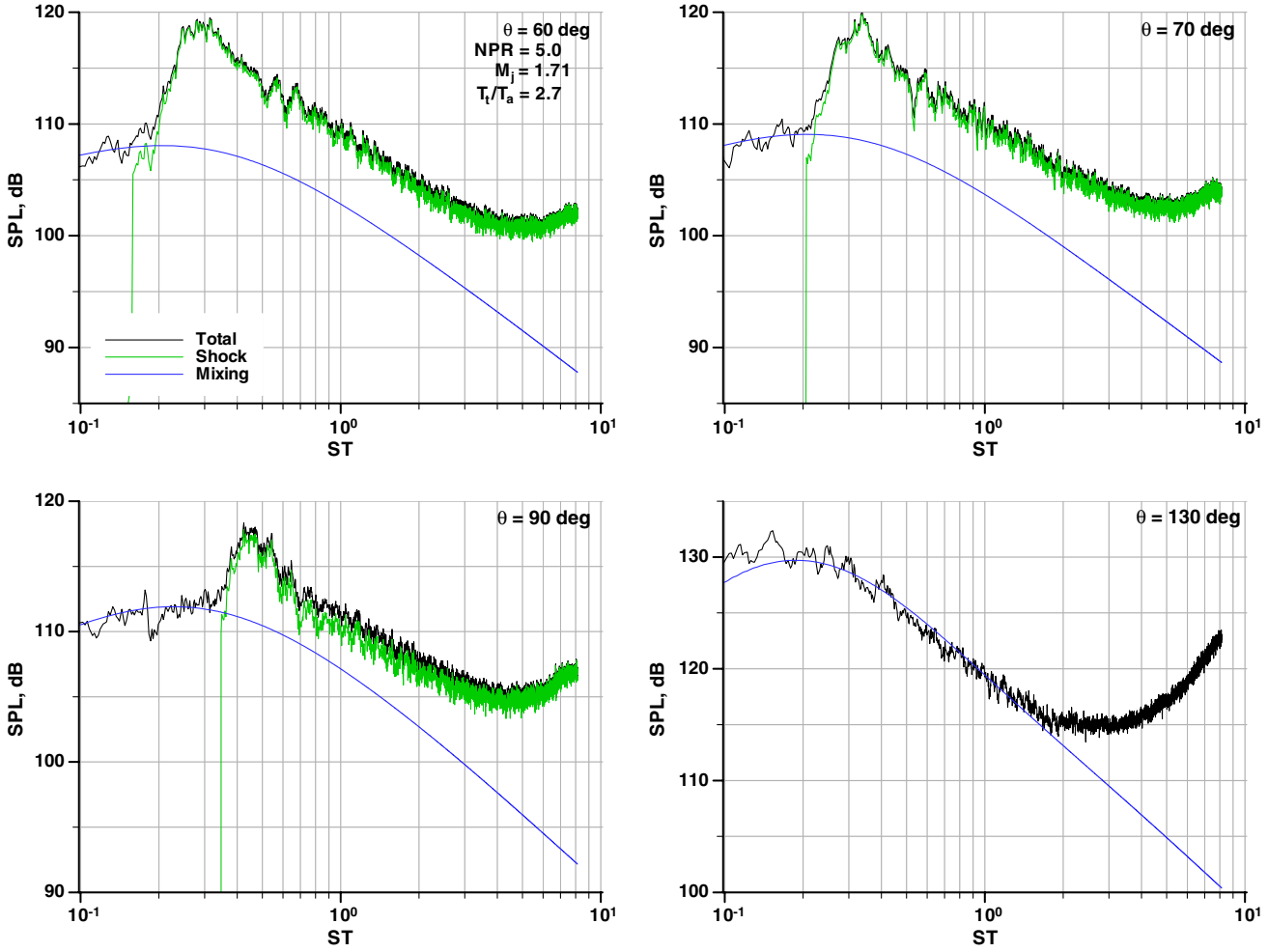

Fig. 34 Comparison of extracted mixing and shock-associated noise normalized to fixed distance; $M = 1.72$, and $T_t/T_a = 2.7$. Black: total, blue: mixing noise, and green: shock noise.

slope of 3.68 is seen to capture the variation of OASPL for the lowest five Mach numbers; there is a saturation of the overall levels for the highest two M_j. Figure 21 shows the curve fits for jets at three different temperature ratios and at three different radiation angles; the values of the shock exponents are also included in this figure. It is evident that the values of the exponents (3.82, 3.31, and 2.62) are much different from 4. The saturation of the OASPL levels at the highest two M_j for the jets with $T_t/T_a = 2.2$ and 2.7 can also be seen in this figure. The exponents thus obtained for all the temperature ratios and all the angles (up to 120 deg) are presented in Fig. 22; least-square fits for the two extreme temperature ratios of 1.0 and 3.2 are also included. At 60 deg, the values of the exponents are close to 4 for all the temperature ratios, in agreement with the past observations of [1,2]. However, the influence of the temperature ratio on the value of the shock exponent becomes apparent as we move aft; there is a clear decrease in the values as the jet temperature is increased. Furthermore, the values keep decreasing with increasing angle, as denoted by the curve fits; the rate of decrease becomes steeper as the temperature is increased. It is obvious from this figure that the exponent with the total OASPL does not have a fixed value of 4. The shock exponent is also seen to have a dependence on the temperature ratio and angle, similar to the trend seen for the mixing noise exponent; see Fig. 16 and associated discussion in [13].

2. *Shock Component Alone*

Next we examine the variation of the shock exponent obtained from the OASPL calculated from the broadband shock component alone. Figure 23 shows typical curve fits for three different conditions; the values of the exponents (4.57, 5.18, and 5.83) are much higher than 4. There is again saturation of the noise levels at the highest two M_j for all the cases shown. The exponents for all the temperature ratios over a range of radiation angles are shown in Fig. 24. The values lie in the range of 2.9–6.17, with most exponents greater than 4; there is no discernible trend as seen for the exponents obtained with the total OASPL. The main new conclusion of this exercise is the following: the value of the shock exponent is not exactly four but has a dependence on jet temperature and radiation angle.

An attempt is made to collapse the spectra with the experimentally-determined exponents to verify if it would be possible to generate universal spectra, as is done for the turbulent mixing noise and illustrated in Figs. 3 and 4. Jets at a fixed stagnation temperature of 3.2 are considered. First, we examine the total spectra and the shock components at an angle of 60 deg in Fig. 25 as a function of raw frequency. As the jet Mach number is increased, there is progressive increase in the noise levels till a strong Mach disk is formed at $M_j = 1.83$. Of greater concern for spectral scaling is the fact that the spectral peak keeps moving to lower frequencies. When the same spectra are plotted against the Strouhal number in Fig. 26, the consequence of the reduction in the peak shock frequency with increasing M_j becomes more apparent, with the shock peaks spread further apart because of the increasing jet velocities. It is immediately evident that the Strouhal number is not the right nondimensional frequency that would align the broadband shock peaks. An alternate nondimensional parameter or a multiplicative factor for the Strouhal number needs to be formulated. This multiplicative factor, for example, can be determined empirically from the measured spectral peaks. Two different modified Strouhal numbers are defined as follows:

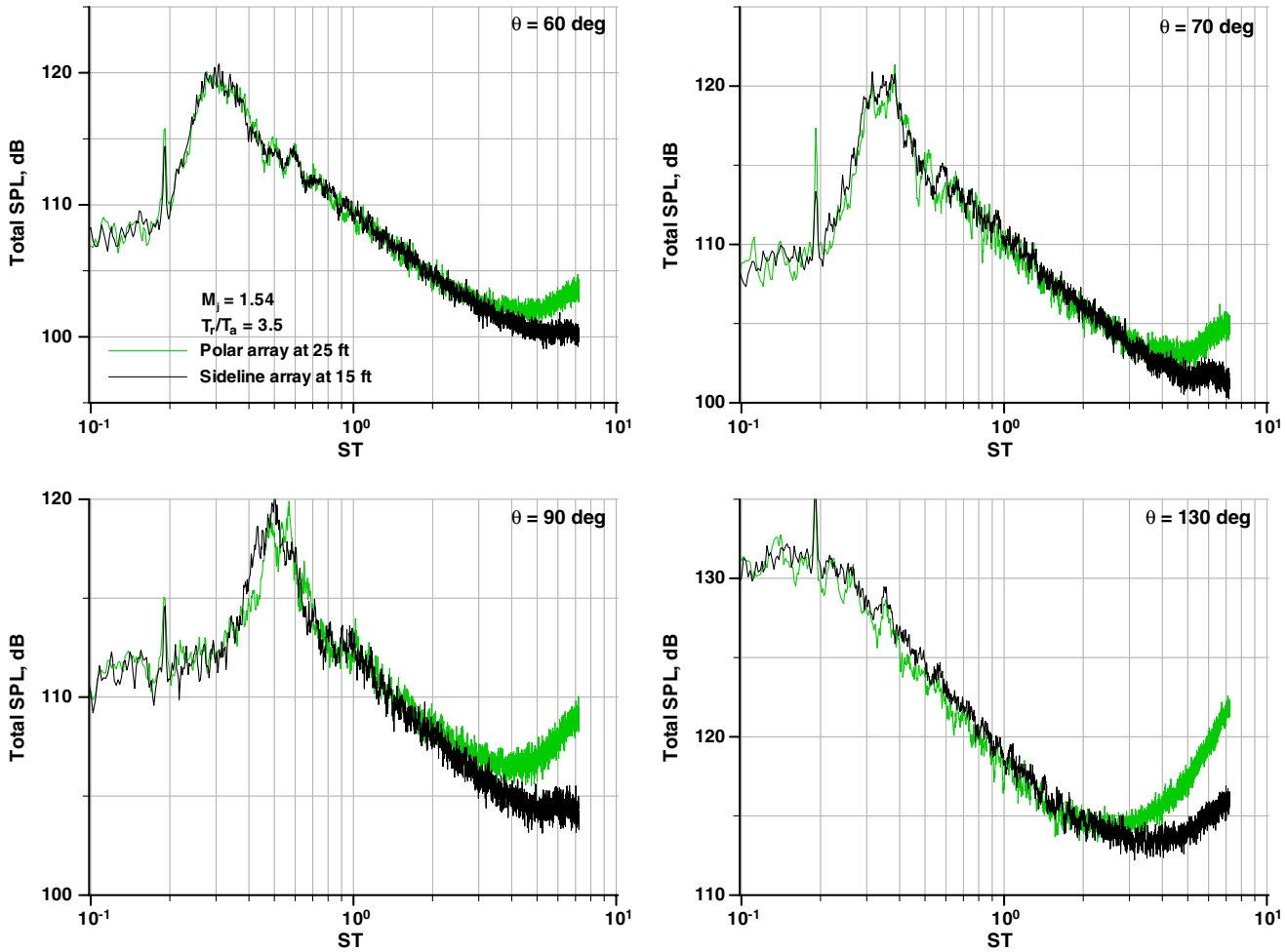

Fig. 35 Comparison of spectra from microphones at different locations normalized to fixed distance; $M = 1.54$, and $T_t/T_a = 3.5$. Green: 25-ft polar, and black: 15-ft constant sideline.

$$St_{\text{mod1}} = \frac{fD_j}{V_j}[1 + \alpha(|M_j^2 - M_D^2|)]$$

$$St_{\text{mod2}} = \frac{fD_j}{V_j}\left[1 + \alpha\sqrt{|M_j^2 - M_D^2|}\right]$$

The spectra at an angle of 60 deg were first collapsed with different values of α. Surprisingly, the value of unity aligns the screech tones perfectly and the broadband peaks for the three higher Mach numbers of 1.37, 1.48, and 1.57 in Fig. 27 when plotted against St_{mod1}. The spectrum from the lower Mach number jet with 1.24 does not have a prominent screech tone and does not line up with the other spectra. Further, there is nonlinear propagation for the higher three Mach numbers, which can be identified with the elevated levels at the high-frequency regime; see Section V.D and Table 1 for more details. A similar alignment of the screech tone and its harmonic for the higher three Mach numbers are also observed for the normalized spectra at 90 deg in Fig. 28. A sample normalized spectral plot with the second modified Strouhal number and at an angle of 60 deg is presented in Fig. 29; the value of α is 20. The agreement for the higher three Mach numbers are comparable to that seen in Fig. 27. In theory, one could find a complicated function that could perhaps provide a better fit but the simplicity of St_{mod1} is more appealing. The main message from this exercise is that it is not straightforward to collapse the shock spectra even for underexpanded jets with fixed $M_d = 1.0$.

D. Nonlinear Propagation Effects for Shock Noise

We examine the spectra from underexpanded jets to discern any nonlinear propagation effects. Two different microphone arrays were deployed: a 25-ft (7.62 m) polar array, and a 15-ft (4.57 m) constant sideline-distance array. The nozzle diameter is 2.45 in. Note that the distance to the microphone changes with the angle for the constant sideline array [equal to $15/\sin(\theta)$]. The nondimensional distance to the polar array is $\sim 122D$. The spectra from the different microphones have been corrected to lossless conditions and extrapolated to a common distance of 20 ft (6.1 m), with the assumption of linear propagation. First, the as-measured spectra from a $M_j = 1.71$ and $T_t/T_a = 3.2$ jet are shown, along with the ambient noise floor levels in Fig. 30, at two angles from the polar array at 25 feet. The noise floor level peaks at 200 Hz and is $\sim$32 dB; the level drops with increasing frequency and reaches $\sim$10 dB for all frequencies $\geq \sim$10 kHz. The spectral levels for jet noise are considerably higher by $\sim$50 dB; similar trends are observed at other angles. Many aspects of the instrumentation system, such as the dynamic range, the microphone corrections, etc., that can lead to turn ups at the higher frequencies are described in Ref. [20]. This figure indicates that the levels at the higher frequencies are well above the noise floor, assuring an excellent signal-to-noise ratio and discounting any potential problems with the instrumentation system for the tail-ups in the spectra.

The spectra from a supersonic jet with a low Mach number of 1.1 at a temperature ratio of 1.8 and an unheated jet with a high Mach number of 1.83 are shown in Figs. 31 and 32, respectively. The convective Mach numbers for these two cases are 0.93 and 0.99, respectively. There is excellent collapse of the two sets of spectra at all angles and all frequencies. Next we consider a jet at a much higher velocity; $M_j = 1.72$ and $T_t/T_a = 2.7$, with $M_c = 1.58$. The normalized spectra are presented in Fig. 33. The trend of increasing sound pressure level at the higher frequencies at 130 deg is expected given the accumulation of energy observed at lower (V_j/a) for the turbulent mixing noise. It is verified in Fig. 34 that the turbulent mixing noise is indeed the dominant component at this angle; the predicted mixing noise component almost fully matches the total measured noise at the spectral peak and at most of the lower frequencies. The lift seen in the spectrum at the higher frequencies is due to nonlinear propagation effects, as discussed previously. Interesting trends are observed at the lower polar angles in Fig. 33; again there is transfer of energy to the high-frequency portion of the spectra, resulting in elevated levels for the farther microphone. It is also clear from Fig. 34 that the shock component is dominant at the higher frequencies at the lower polar angles. This observation establishes that nonlinear propagation effects, whereby there is

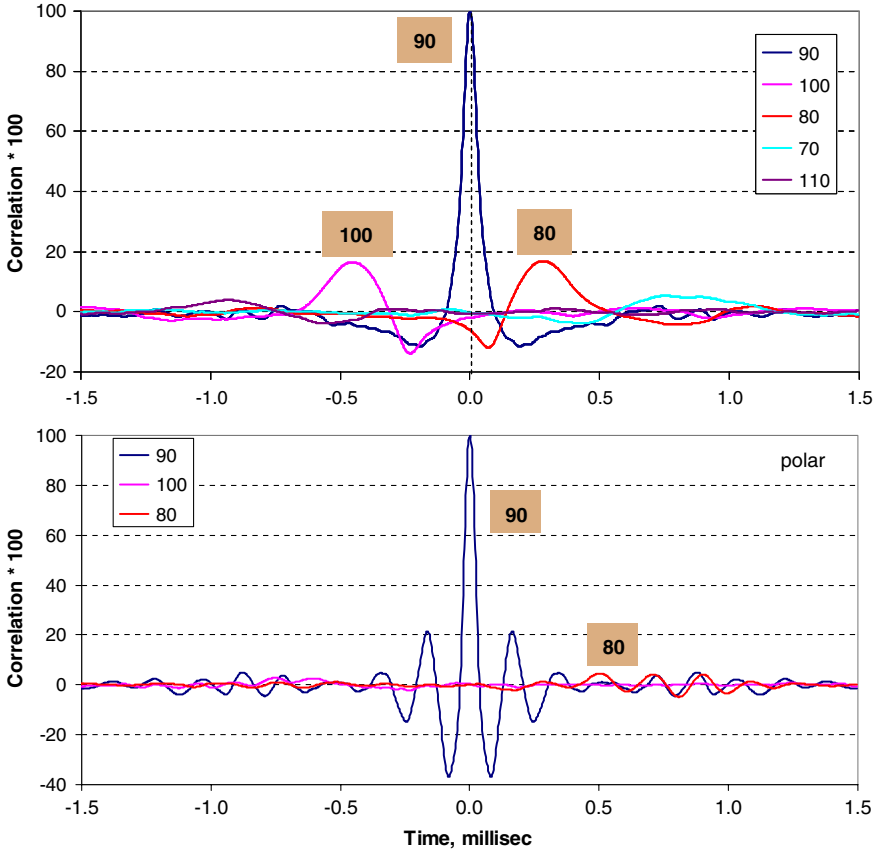

Fig. 36 Polar correlation coefficient with reference microphone at 90 deg; $T_t/T_a = 3.2$. Top: $M = 0.9$, and bottom: $M = 1.57$.

transfer of energy to the higher frequencies with increasing propagation distance, is also manifested for shock noise. Another example of the observed nonlinear effects for the shock component is shown in Fig. 35; $M_j = 1.54$ and $T_t/T_a = 3.5$ for this case.

After this discovery, the entire database was examined to uncover the influence, if any, of M_c and the OASPL on the onset of nonlinear propagation effects. It is well known that the peak noise radiation is at an angle of 150 deg for unheated and heated subsonic jets, and that the peak radiation moves to lower angles for supersonic heated jets. For the heated jets at higher Mach numbers considered here, the peak angle is at $\sim$125 deg; see Fig. 18. It is also established that the nonlinear effects are confined to a polar angular region $\geq \sim$125 deg, for the turbulent mixing noise from highly heated subsonic jets. We consider an angle of 60 deg, to avoid any ambiguity that the observed agglomeration of energy at the higher frequencies could be for the mixing noise and not the shock noise for these highly heated supersonic jets. Figure 34 provides clear-cut evidence that the shock noise is the dominant component at the higher frequencies at 60 deg.

Table 1 provides the jet operating conditions, M_c, and the OASPL at 60 deg at a nondimensional distance (r/D) of $\sim$95; the presence or absence of nonlinear propagation for all the cases is also indicated in this table. The main trends are first identified: 1) there is no nonlinear propagation for all unheated jets; 2) there is no nonlinear propagation for the $M_j = 1.1$ jet at all temperature ratios; 3) there is nonlinear propagation for all heated jets with $M_j \geq 1.38$; 4) M_c is not a good indicator of the onset of nonlinear propagation effects: compare $M_j = 1.24$, $T_t/T_a = 3.14$, $M_c = 1.34$ (linear) with $M_j = 1.83$, $T_t/T_a = 1.8$, $M_c = 1.28$ (nonlinear); and 5) the OASPL is also not a good indicator of the onset of nonlinear propagation effects: compare $M_j = 1.83$, $T_t/T_a = 1.0$, OASPL = 98.0 dB (linear) with $M_j = 1.38$, $T_t/T_a = 3.51$, OASPL = 97.1 dB (nonlinear). It is not clear at this point what physical phenomenon triggers the onset of nonlinear propagation for the shock noise. Seiner et al. [24] reported the absence of any evidence for significant nonlinear effects from a full-scale static test of the F404-400 engine; see figure 11 in this reference. The jet operating conditions are not given, but it is surmised that they are probably within the conditions in Table 1 for which linear propagation results.

E. Far-field Correlations of Shock Noise

Far-field correlations of jet noise have recently been measured with a fixed polar array and a traversing azimuthal array. Detailed descriptions of the two arrays, the measurement and data processing

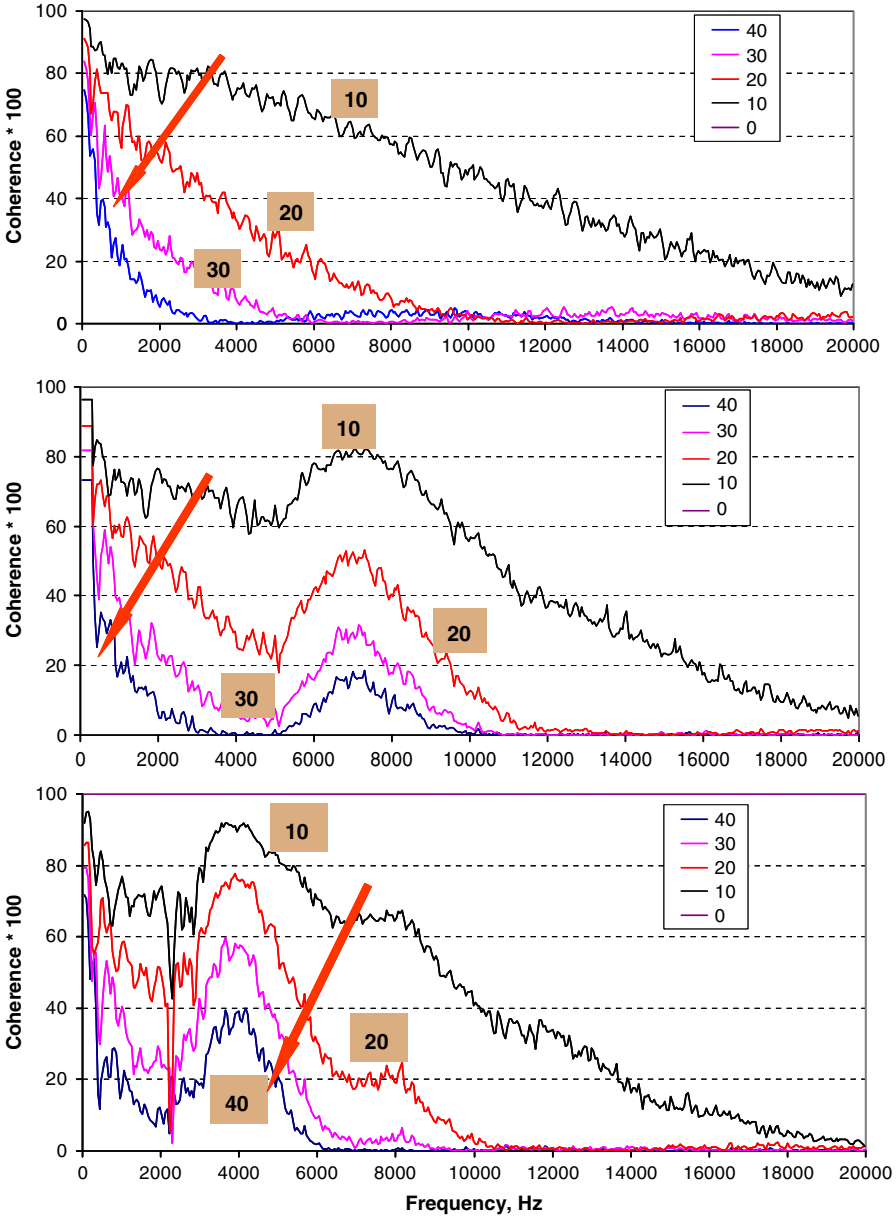

Fig. 37 Comparison of azimuthal coherence spectra for different microphone separation angles; $T_t/T_a = 3.2$, and polar angle = 90 deg. Top: $M = 0.9$, middle: $M = 1.24$, and bottom: $M = 1.57$.

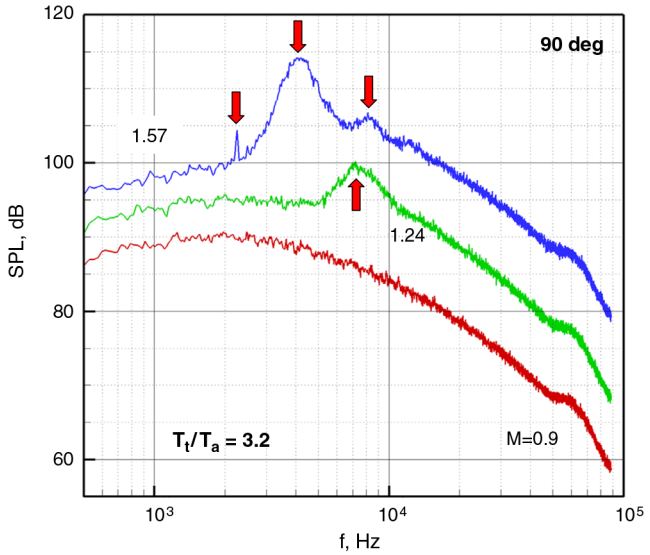

Fig. 38 Comparison of far-field spectra; $T_t/T_a = 3.2$, and polar angle = 90 deg. Bottom: $M = 0.9$, middle: $M = 1.24$, and top: $M = 1.57$.

techniques, etc., are provided in Viswanathan [25]. The salient correlation results for the turbulent mixing noise are also presented in Viswanathan [25]. The signals from the array microphones are time synchronized; because the distances to the microphones in each array have a fixed value, no corrections related to the weather conditions are applied in the processing of the correlation data. The time-series data have been processed to produce some basic correlation plots and coherence spectra. The coherence function $\gamma^2(f)$ between any two microphones is defined by

$$\gamma_{12}^2(f) = \frac{|G_{12}(f)|^2}{G_{11}(f)G_{22}(f)}$$

where G_{11} and G_{22} are the one-sided autospectra, and G_{12} is the cross spectrum between the two signals. Similarly, the cross-correlation coefficient function $\eta_{12}(\tau)$ is defined by

$$\eta_{12}(\tau) = \frac{R_{12}(\tau)}{\sqrt{R_{11}(0)}\sqrt{R_{22}(0)}}$$

where R_{11} and R_{22} are the autocorrelation functions, R_{12} is the cross-correlation function, and τ represents the time delay.

The correlation coefficients and coherence spectra at an angle of 90 deg are presented for jets with Mach numbers of 0.9, 1.24, and 1.57; the temperature ratio for all the jets is 3.2. The subsonic case is included to contrast between the different noise generation mechanisms and how they affect the behavior of the correlations. The polar correlation coefficients for the $M_j = 0.9$ and 1.57 jets are shown in Fig. 36. The autocorrelation coefficient at 90 deg has the expected value of unity for zero time separation. For the subsonic case, the levels of the maximum correlation coefficient drop to less than 0.2 for a separation angle of ± 10 deg. For the supersonic case, there is no appreciable level for the cross-correlation coefficient for any time separation for the microphones which are at ± 10 deg from the reference microphone; in fact, the values are close to zero. However, the more interesting aspect is seen in the shapes of the autocorrelation functions. Attention is drawn to the deep and large negative peaks for the supersonic jet. Tam et al. [26] explained the reason for the appearance of these negative loops and pictorially illustrated the role of the large scale coherent structures in the formation of these negative peaks; see section III in Ref. [26]. The noise at 90 deg for the subsonic jet is generated by the fine-scale turbulence, which does not form large negative loops in the autocorrelation function. As noted earlier, broadband shock-associated noise is generated by the interaction of the downstream-convecting coherent structures of the jet flow with the shock cells in the jet plume. The observation of the negative peaks points to the role of the large coherent structures in the physical mechanism responsible for shock noise generation.

Figure 37 shows the azimuthal coherence spectra for different microphone pairs with increasing separation angle in the azimuthal direction, in the frequency range of 400 Hz to 20 KHz. The angular separations in the azimuthal plane are denoted in these plots. The autocoherence functions have a value of unity at all frequencies and are denoted by straight horizontal lines. For the subsonic jet, the values of the coherence drop sharply with increasing separation angle and increasing frequency. This trend is consistent with noise generated by random and uncorrelated fine-scale turbulence. The

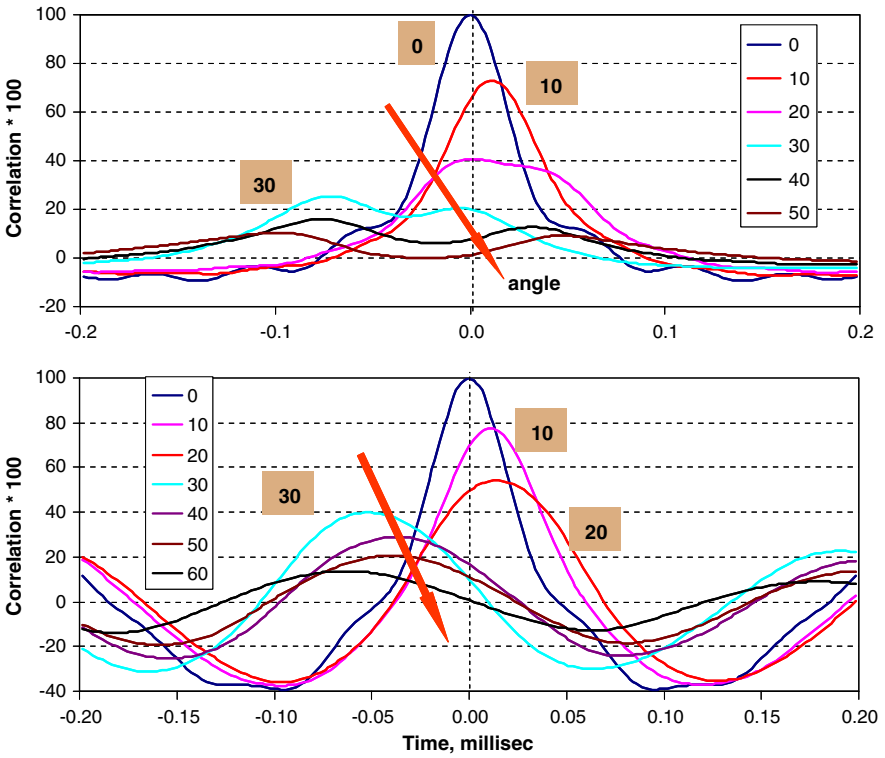

Fig. 39 Azimuthal correlation coefficients with azimuthal array positioned at polar angle of 90 deg; $T_t/T_a = 3.2$. Top: $M = 0.9$, and bottom: $M = 1.57$.

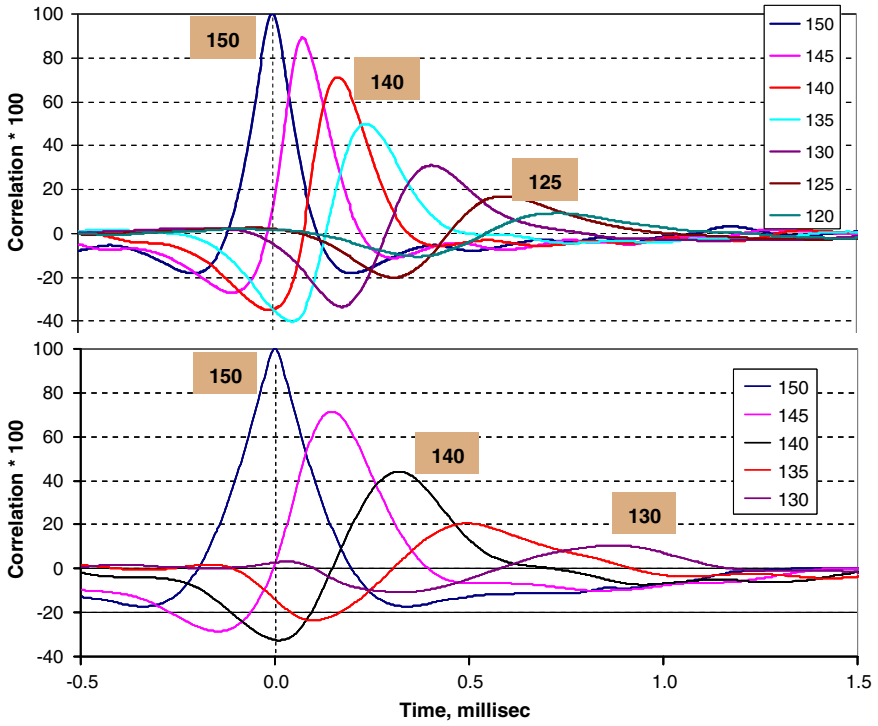

Fig. 40 Polar correlation coefficients with reference microphone at 150 deg; $T_t/T_a = 3.2$. Top: $M = 0.9$, and bottom: $M = 1.57$.

coherence functions for the supersonic jets are drastically different from those for the subsonic jet; the coherence values initially decrease with increasing frequency, but a well marked peak at a frequency of ~7100 Hz is observed for the $M_j = 1.24$ jet. For the $M_j = 1.57$ jet, three distinctive features can be identified: a sharp dip at ~2250 Hz, a major peak at ~4100 Hz, and a second peak at ~8100. The corresponding far-field spectra at 90 deg for the three Mach numbers are presented in Fig. 38. The subsonic spectrum has the typical broad shape seen for the turbulent mixing noise at the lower radiation angles. For the $M_j = 1.24$ jet, the broadband shock noise has a peak at ~7100 Hz; this peak appears as a peak at the same frequency in the coherence spectrum. The following features can be identified for the $M_j = 1.57$ jet: 1) a screech tone at ~2250 Hz, 2) a strong broadband peak at ~4100 Hz, and (3) a secondary peak at ~8100 Hz. All these peaks are identified by arrows in this figure. It is clear that the peaks associated with the shock noise in the far field are imprinted with corresponding features on the coherence spectra. This result once again confirms the role of a coherent source on the generation of shock noise.

The azimuthal correlation coefficients for the $M_j = 0.9$ and 1.57 jets at a polar angle of 90 deg are examined in Fig. 39. For the subsonic jet, the levels fall below 0.20 for a separation angle of 40 deg. For the $M_j = 1.57$ jet, the functions have completely different shapes, with large negative peaks. Furthermore, the levels of the peak correlation coefficients remain at ~0.20 for a larger separation angle of 60 deg. The large negative loops again indicate a different noise mechanism that involves the large coherent structures in the generation of shock noise. For the sake of completeness, the polar correlation coefficients for the $M_j = 0.9$ and 1.57 jets with the reference microphone at 150 deg are shown in Fig. 40. The trends for the two cases are quite similar, except for the larger half-width for the autocorrelation function for the supersonic jet. Of course, the observed similarities are expected because the turbulent mixing noise is the dominant component at this aft angle.

VI. Conclusions

The characteristics of the broadband shock-associated noise are examined in this study. The mixing and broadband shock components are first extracted from the total spectra. This decomposition is made possible by a recently developed scaling methodology for turbulent mixing noise, which provides excellent collapse of the mixing noise spectra from jets at all velocities but at a fixed temperature ratio. The examination of the shock component alone reveals the following characteristics:

1) The levels for the shock and mixing components are comparable for moderately offdesign highly heated jets.

2) There is a clear effect of jet temperature on shock noise. The levels increase as the jet is first heated; however, the levels do not increase with further increase in jet temperature. The physical phenomenon responsible for this saturation of levels is not known at this time.

(3) The directivity curves for the shock OASPL are flat, confirming the omni-directional nature of shock noise.

(4) As already established, the intensity of shock-associated noise is strongly influenced by the degree of imperfect expansion, quantified by the parameter (β)

$$\sqrt{|M_j^2 - M_D^2|}$$

5) The exponent of β for shock intensity is not exactly 4, but spans a range from 2.9 to 6.17, depending on the radiation angle and the jet temperature ratio.

The Strouhal number does not collapse the shock spectra from jets with different Mach numbers. A modified Strouhal number is introduced and is shown to provide a reasonable collapse of the spectra when used in conjunction with the experimentally-determined exponent for shock intensity. It is also established for the first time that nonlinear propagation effects are manifested at lower radiation angles, in which the shock component is dominant. However, the physical phenomenon that triggers the onset of nonlinear propagation for the shock noise could not be identified. Neither the convective Mach number nor the OASPL at a particular angle is a good indicator for the presence of nonlinear propagation. The situation is different from that for the turbulent mixing noise, in which the convective Mach number of unity defines the boundary between linear and nonlinear propagation.

The coherence and correlation coefficient functions for the supersonic jets are different from their subsonic counterparts. At the lower angles, the spectra for subsonic jets are generated by the random turbulence; the correlations are very low given the nature of the noise

source. In contrast, the azimuthal coherence functions for the shock-dominated spectra for the supersonic jets have distinctive features, the frequencies of which correspond to the broadband shock peak and the screech tone in the far field. Further, the correlation functions display large negative loops, which are associated with noise generated by large coherent structures. The occurrence of these negative peaks indicates the role of the large coherent structures in the generation of the broadband shock-associated noise. Thus, the vastly different noise mechanisms at the lower radiation angles for the subsonic and shock-containing supersonic jets leave their distinctive imprints on the correlation functions.

References

[1] Harper-Bourne, M., and Fisher, M. J., "The Noise from Shock Waves in Supersonic Jets," AGARD CP-131, 1973, pp. 1–13.

[2] Tanna, H. K., "An Experimental Study of Jet Noise. Part II: Shock Associated Noise," *Journal of Sound and Vibration*, Vol. 50, No. 3, 1977, pp. 429–444.
doi:10.1016/0022-460X(77)90494-1

[3] Seiner, J. M., and Norum, T. D., "Experiments on Shock Associated Noise of Supersonic Jets," AIAA Paper 79-1526, 1979.

[4] Seiner, J. M., and Norum, T. D., "Aerodynamic Aspects of Shock Containing Jet Plumes," AIAA Paper 80-0965, 1980.

[5] Norum, T. D., and Seiner, J. M., "Measurements of Static Pressure and Far Field Acoustics of Shock-Containing Supersonic Jets," NASA TM 84521, 1982.

[6] Norum, T. D., and Seiner, J. M., "Broadband Shock Noise from Supersonic Jets," *AIAA Journal*, Vol. 20, No. 1, 1982, pp. 68–73.
doi:10.2514/3.51048

[7] Tam, C. K. W., and Tanna, H. K., "Shock Associated Noise of Supersonic Jets from Convergent-Divergent Nozzles," *Journal of Sound and Vibration*, Vol. 81, No. 3, 1982, pp. 337–358.
doi:10.1016/0022-460X(82)90244-9

[8] Seiner, J. M., "Advances in High Speed Jet Aeroacoustics," AIAA Paper 84-2275, 1984.

[9] Seiner, J. M., and Yu, J. C., "Acoustic Near-Field Properties Associated with Broadband Shock Noise," *AIAA Journal*, Vol. 22, No. 9, 1984, pp. 1207–1215.
doi:10.2514/3.8762

[10] Yamamoto, K., Brausch, J. F., Janardan, B. A., Hoerst, D. J., Price, A. O., and Knott, P. R., "Experimental Investigation of Shock-Cell Noise Reduction for Single-Stream Nozzles in Simulated Flight," *Test Nozzles and Acoustic Data, Comprehensive Data Report*, Vol. 1, NACA CR-168234, May 1984.

[11] Tam, C. K. W., "Stochastic Model Theory of Broadband Shock Associated Noise from Supersonic Jets," *Journal of Sound and Vibration*, Vol. 116, No. 2, 1987, pp. 265–302.
doi:10.1016/S0022-460X(87)81303-2

[12] Tam, C. K. W., "Jet Noise Generated by Large-Scale Coherent Motion," in *Aeroacoustics of Flight Vehicles: Theory and Practice, Volume 1: Noise Sources*, edited by H. H. Hubbard, NASA RP-1258, 1991, pp. 311–390.

[13] Viswanathan, K., "Scaling Laws and a Method for Identifying Components of Jet Noise," *AIAA Journal*, Vol. 44, No. 10, Oct. 2006, pp. 2274–2285.
doi:10.2514/1.18486

[14] Viswanathan, K., "Improved Method for Prediction of Noise from Single Jets," *AIAA Journal*, Vol. 45, No. 1, 2007, pp. 151–161.
doi:10.2514/1.23202

[15] Tam, C. K. W., Golebiowski, M., and Seiner, J. M., "On the Two Components of Turbulent Mixing Noise from Supersonic Jets," AIAA Paper 96-1716, 1996.

[16] Viswanathan, K., and Czech, M. J., "Role of Jet Temperature in Correlating Jet Noise," *AIAA Journal*, Vol. 47, No. 5, May 2009, pp. 1090–1106.
doi:10.2514/1.35718

[17] Shields, F. D., and Bass, H. E., "Atmospheric Absorption of High Frequency Noise and Application to Fractional-Octave Band," NASA CR 2760, 1977.

[18] Viswanathan, K., "Does a Model Scale Nozzle Emit the Same Jet Noise as a Jet Engine?" *AIAA Journal*, Vol. 46, No. 2, Feb. 2008, pp. 336–355.
doi:10.2514/1.18019

[19] Viswanathan, K., "Jet Aeroacoustic Testing: Issues and Implications," *AIAA Journal*, Vol. 41, No. 9, 2003, pp. 1674–1689.
doi:10.2514/2.7313

[20] Viswanathan, K., "Instrumentation Considerations for Accurate Jet Noise Measurements," *AIAA Journal*, Vol. 44, No. 6, June 2006, pp. 1137–1149.
doi:10.2514/1.13518

[21] Viswanathan, K., "Recent Advances in Jet Noise Suppression," *International Symposium on Recent Advances in Aeroacoustics and Active Flow-Combustion Control*, Goa, India, Jan. 2005 (unpublished).

[22] Saxena, S., Morris, P. J., and Viswanathan, K., "A New Algorithm for the Nonlinear Propagation of Broadband Jet Noise," *AIAA Journal*, Vol. 47, No. 1, Jan. 2009, pp. 186–194.
doi:10.2514/1.38122.

[23] Viswanathan, K., Shur, M., Spalart, P. R., and Strelets, M. K., "Flow and Noise Predictions for Single and Dual-Stream Beveled Nozzles," *AIAA Journal*, Vol. 46, No. 3, 2008.
doi:10.2514/1.27299

[24] Seiner, J. M., Ukeiley, L. S., and Jansen, B. J., "Aero-Performance Efficient Noise Reduction for the F404-400 Engine," AIAA Paper 2005-3048, May 2005.

[25] Viswanathan, K., "Investigation of Noise Source Mechanisms in Subsonic Jets," *AIAA Journal*, Vol. 46, No. 8, Aug. 2008, pp. 2020–2032.
doi:10.2514/1.34471; also see AIAA Paper 2007-3601, May 2007).

[26] Tam, C. K. W., Viswanathan, K., Ahuja, K. K., and Panda, J., "The Sources of Jet Noise: Experimental Evidence," *Journal of Fluid Mechanics*, Vol. 615, 2008, pp. 253–292.
doi:10.1017/S0022112008003704

E. Gutmark
Associate Editor